11900–11919 *Nucleic Acids Research, 2021, Vol. 49, No. 20* *Published online 20 October 2021*
https://doi.org/10.1093/nar/gkab927

THUMPD3–TRMT112 is a m^{2}G methyltransferase working on a broad range of tRNA substrates

Wen-Qing Yang[1], Qing-Ping Xiong[2], Jian-Yang Ge[1], Hao Li[1], Wen-Yu Zhu[1], Yan Nie[3], Xiuying Lin[4], Daizhu Lv[5], Jing Li[1], Huan Lin[4] and Ru-Juan Liu[1,*]

[1]School of Life Science and Technology, ShanghaiTech University, Shanghai 201210, China, [2]CAS Center for Excellence in Molecular Cell Science, Shanghai Institute of Biochemistry and Cell Biology, Chinese Academy of Sciences; University of Chinese Academy of Sciences, Shanghai 200031, China, [3]Shanghai Institute for Advanced Immunochemical Studies, ShanghaiTech University, Shanghai 201210, China, [4]State Key Laboratory of Marine Resource Utilization in South China Sea, Hainan University, Haikou, China and [5]Analysis and Testing Center, Chinese Academy of Tropical Agricultural Sciences, Haikou 571101, China

Received July 06, 2021; Revised September 06, 2021; Editorial Decision September 23, 2021; Accepted October 08, 2021

ABSTRACT

Post-transcriptional modifications affect tRNA biology and are closely associated with human diseases. However, progress on the functional analysis of tRNA modifications in metazoans has been slow because of the difficulty in identifying modifying enzymes. For example, the biogenesis and function of the prevalent N2-methylguanosine (m^{2}G) at the sixth position of tRNAs in eukaryotes has long remained enigmatic. Herein, using a reverse genetics approach coupled with RNA-mass spectrometry, we identified that THUMP domain-containing protein 3 (THUMPD3) is responsible for tRNA: m^{2}G6 formation in human cells. However, THUMPD3 alone could not modify tRNAs. Instead, multifunctional methyltransferase subunit TRM112-like protein (TRMT112) interacts with THUMPD3 to activate its methyltransferase activity. In the *in vitro* enzymatic assay system, THUMPD3–TRMT112 could methylate all the 26 tested G6-containing human cytoplasmic tRNAs by recognizing the characteristic 3′-CCA of mature tRNAs. We also showed that m^{2}G7 of tRNA^{Trp} was introduced by THUMPD3–TRMT112. Furthermore, THUMPD3 is widely expressed in mouse tissues, with an extremely high level in the testis. *THUMPD3*-knockout cells exhibited impaired global protein synthesis and reduced growth. Our data highlight the significance of the tRNA: m^{2}G6/7 modification and pave a way for further studies of the role of m^{2}G in sperm tRNA derived fragments.

INTRODUCTION

Post-transcriptional modifications are frequently introduced in RNA molecules by the activity of modifying enzymes. To date, almost 170 types of chemical modification have been found in coding and non-coding RNAs across all domains of life (1). Among them, transfer RNA (tRNA) has been identified as one of the most modified cellular RNAs (2–5). As adaptor molecules between messenger RNA (mRNA) and amino acids, modifications of tRNAs help to ensure the stability of tRNA structure (6), the fidelity of protein synthesis (7) and the degeneracy of coding sequences (8). In addition, tRNA modifications are related to the generation of tRNA-derived fragments (tRFs) (9), immune responses (10), homeostasis (11) and intergenerational inheritance (12). Moreover, aberrant tRNA modification is strongly associated with various human diseases (13–15).

To gain a deeper insight into the functions and physiological roles of those chemical modifications of tRNAs, it is essential to characterize their modifying enzymes. Nevertheless, although most of the tRNA modifications were identified several decades ago (16), the work of identifying modifying enzymes lags far behind. Up to now, a quarter of genes encoding the human tRNA modifying proteins remain to be discovered (5). The difficulty of identifying the enzymes responsible for tRNA modifications in higher eukaryotes stems mainly from the following aspects: (i) It is hard to predict tRNA modification enzyme genes based on their prokaryotic homologs. The same tRNA modifications could be generated by uncorrelated proteins from evolutionarily different resources. For example, both TrmD and Trm5 could be responsible for m^{1}G37 formation, although they evolved from completely different resources in bacteria and archaea/eukaryotes (17). (ii) It is difficult to reconstitute the *in vitro* enzymatic activity of putative

*To whom correspondence should be addressed. Tel: +86 21 20684574; Fax: +86 21 20685430; Email: liurj@shanghaitech.edu.cn

eukaryotic modification enzymes (18). Firstly, it was difficult to produce the functional proteins *in vitro*. Secondly, many modifying enzymes in eukaryotes need auxiliary proteins to complete their catalytic role. For example, TrmL in bacteria can independently catalyze 2′-*O*-methylation (Nm) of tRNA at position 34 (19); however, the eukaryotic Trm7 of yeast needs to be in complex with Trm732 or Trm734 to form Nm in tRNAs at positions 32 or 34 (20). Lastly, in the complicate network of tRNA modifications, some modifications must be established based on the existence of other pre-modified nucleosides. For example, i^6A37 is a prerequisite for Nm at position 34 of *Escherichia coli* $tRNA^{Leu}$ (21). (iii) High throughput methods to identify RNA modifications at single base resolution are limited to few types, and it remains to be developed to excavate the vast majority of the RNA modifications (22,23).

The addition of methyl groups to bases of nucleosides is the most common RNA modification (24,25). Methylation of the amino group at the C2 position of guanine forms N2-methylguanosine (m^2G) or N2,N2-dimethylguanosine ($m^2{}_2G$), both of which are prevalent modifications of RNAs. The presence of $m^2{}_2G$ blocks G-C base pairing during reverse transcription, and thus could be detected using high throughput sequencing (26,27). However, there is no available high-throughput sequencing-based method to detect m^2G. The m^2G modification of tRNA molecule is widespread and conserved in eukaryotes, archaea, and some bacteria. Interestingly, the level of m^2G in tRNA was observed to be dynamic during the cellular stress response in yeast (28). In particular, the level of m^2G was decreased significantly after exposure to H_2O_2. Recently, it was reported that m^2G and m^5C (5-methylcytidine) are the two modifications that increased remarkably in sperm tRFs of high fatty diet (HFD) group, which mediate the intergenerational inheritance from parental mice to their offspring (29). The biogenesis and biological significance of the m^5C of tRNAs and the related tRFs have been studied extensively (30,31); however, the specific role of m^2G modification in tRNAs/tRFs remains unknown, especially in mammals.

The m^2G modification is distributed widely in tRNAs, such as at positions 6, 7, 8, 9, 10, 26 and 27 (32–36). However, they occur more frequently at two positions: m^2G6 and m^2G10 (33,34), and the remaining such modifications are distributed sporadically in specific kinds of tRNAs. Interestingly, m^2G mainly occurs in the 5′-half of tRNA molecules, which is the main source of 5′-tRF that is dominantly present in the cellular tRF pool (37). G26 in tRNAs is also frequently methylated; however, G26 was predominantly modified into $m^2{}_2G26$ by Trm1 in most cytoplasmic tRNAs (35). The $m^2{}_2G26$ modification was reported to act as a molecular hinge to adjust the tRNA architecture and correlates with the thermostability of specific tRNAs (38,39). Loss-of-function mutations in *Trmt1* were reported to be related to neurological diseases (40). In eukaryotes, tRNA:m^2G10 is catalyzed by Trmt11 (named as Trm11 in yeast). No remarkable growth defect was observed in yeast deleted for *Trm11* (34), while in the archaeon *Thermococcus kodakarensis*, Trm11 was found to be indispensable for cell survival at high temperatures, and m^2G10 was found to be further modified into $m^2{}_2G10$ in this species (41). In eukaryotes, the catalytic mechanism of m^2G10 formation has been studied extensively, and an auxiliary protein, Trm112, was identified to assist the catalysis of Trm11 (42). However, the physiological functions of m^2G10 in eukaryotes are largely unknown. The m^2G6 modification is present in almost all sequenced cytoplasmic tRNAs with G6 in mammals, suggesting that this modification is extremely conserved and widespread in mammals (1). Notably, m^2G6 occurs in the acceptor-stem region of the tRNA molecule, which is a rarely modified region. The tRNA:m^2G6 modification is not present in fungi or most bacteria. However, it does occur in some archaea and *Thermus thermophilus (Tt)* (33,43,44), in which it is introduced by methyltransferases (MTases) Trm14 (in archaea) and TrmN (in *Tt*) (33,44). However, the biogenesis and function of tRNA:m^2G6 in eukaryotes are unknown, mainly because the corresponding modifying enzyme has not been identified.

In the present study, we investigated the biogenesis and biological role of tRNA:m^2G6 in human cells. First, we tried to identify the modifying enzyme of tRNA:m^2G6. From protein primary sequence alignment, no highly homologous protein to Trm14 or TrmN was identified in highly eukaryotes. The sequence similarity of archaeal Trm14 and TrmN is also quite low; however, their tertiary structures are quite similar (33,44). They both contain two main domains: a THUMP domain followed by a S-adenosylmethionine (SAM)-dependent Rossman-Fold MTase (RFM) domain. The THUMP domain is an ancient RNA-binding domain, which was named after THioUridine synthase, MTase and Pseudouridine synthase (45). This domain architecture of a THUMP domain followed by an MTase domain is also present in Trm11 (42,46), although with many differences in structural details. In higher eukaryotes, besides Trmt11, another two uncharacterized THUMP domain containing proteins, THUMPD2 and THUMPD3, are predicted to have a similar domain architecture (https://prosite.expasy.org/prosite.html). Considering the functional relevance of tRNA:m^2G modification for TrmN, Trm14, and Trm11, we hypothesized that THUMPD2 and/or THUMPD3 might be the tRNA:m^2G6 MTases in eukaryotes. Actually, a recent bioinformatic analysis survey also suggested THUMPD2 and THUMPD3 as the potential candidates for the tRNA:m^2G6 MTases (5).

Here, using a reverse genetics approach coupled with RNA-mass spectrometry, we identified that THUMPD3 is responsible for $m^2G6/7$ formation of tRNAs in human cells. Nevertheless, unlike TrmN or Trm14, THUMPD3 alone could not catalyze tRNA methylation independently. We further identified that TRMT112, a universal activator for both RNA and protein MTases, could activate the tRNA methyltransferase activity of THUMPD3. We further reconstituted the formation of m^2G6 in human cytoplasmic tRNAs *in vitro*, and found that the THUMPD3–TRMT112 complex has a broad specificity for all the 26 tested G6-containing tRNAs recognizing the characteristic 3′-CCA end. Additionally, THUMPD3–TRMT112 could catalyze m^2G7 on $tRNA^{Trp}$. However, 5′-tRNA-derived fragments (5′-tRFs) and mini-helix of substrate tRNAs could not be catalyzed because the mature tertiary structure of tRNA was also indispensable for recognition by

THUMPD3. We also showed that THUMPD3 is widely distributed in various human cell lines and mouse tissues. Lastly, *THUMPD3*-knockout HEK293T cells exhibited reduced global protein translation and inhibited cell proliferation.

MATERIALS AND METHODS

Materials

Adenosine (A), guanosine (G), cytidine (C), uridine (U), m^2G, $m^2{}_2G$, Ammonium acetate (NH_4OAc), 5′-guanosine monophosphate (GMP), Tris base, β-mercaptoethanol (β-Me), Benzonase, Pyrophosphate, Phosphodiesterase I, Sodium acetate (NaAc), Trypan Blue Stain 0.4%, and RIPA lysis Buffer (10×) were purchased from Sigma Aldrich. Sinefungin (SFG) was purchased from Santa Cruz Biotechnology. CCK-8 Cell Counting Kit, HiScript III RT SuperMix for QPCR (+gDNA wiper), and ChamQ Universal SYBR QPCR Master Mix universal were purchased from Vazyme Biotech. Ribolock RNase inhibitor, Lipofectamine 2000, T4 DNA ligase, Streptavidin-conjugated agarose beads, 4′,6-diamidino-2-phenylindole (DAPI), restriction endonucleases, Pierce Silver Stain Kit, and Polyvinylidene fluoride (PVDF) membranes were purchased from Thermo Fisher Scientific. TRNzol Universal reagent was purchased from Tiangen Biotech. Ni^{2+}-NTA Superflow resin was purchased from Qiagen. Alkaline phosphatase (Calf intestine) was purchased from Takara Biomedical Technology. KOD-Plus-Neo Kit was purchased from TOYOBO Biotech. 1 M Tris–HCl Solution (Sterile), NaCl, $MgCl_2$, ATP, GTP, CTP, UTP, and isopropyl-D-thiogalactoside (IPTG) were purchased from Sangon Biotech. Anti-HA and anti-Flag magnetic beads were purchased from MedChemExpress. X-tremeGENE™ 9 DNA transfection reagent was purchased from Roche. Peroxidase-AffiniPure goat anti-rabbit/mouse IgG(H + L) and cycloheximide (CHX) were purchased from Yeasen. S-adenosylmethionine (SAM) was purchased from New England Biolabs. 5′-Biotin-DNA primers were purchased from BioSune. PCR or qRT-PCR primers were purchased from Tsingke Biological Technology. The antibodies used in this study were purchased from different companies and listed as follows: anti-HA antibody (3724, Cell Signaling Technology), anti-Flag antibody (14793, Cell Signaling Technology), and anti-Histone H3 (9715, Cell Signaling Technology). Alexa Fluor 488 AffiniPure Goat Anti-Rabbit IgG (33106ES60, Yeasen), anti-THUMPD3 antibody (A10407, ABclonal), anti-TRMT112 antibody (A14310, ABclonal), anti-β-Tubulin (A12289, ABcloanal), and anti-GAPDH (AC002, ABclonal).

Cell culture

HeLa cells and HEK293T cells were purchased from the cell resource centre of the Shanghai Institutes for Biological Sciences, Chinese Academy of Sciences, Shanghai, China. All of them were cultured at 37°C with 5% CO_2 in Dulbecco's modified Eagle's medium (DMEM, Corning) supplemented with 10% fetal bovine serum (Lonsera). The viable cell numbers were counted by 0.4% trypan blue staining assays. Insect cells, *Spodoptera frugiperda* Sf9 and High Five cells, were cultured on a shaking incubator at 27°C and 120 rpm in ESF921 medium (Expression Systems).

Plasmids

The coding sequences of human *THUMPD3* (NM_015453.3) and *TRMT112* (NM_016404.3) were amplified from cDNA, which was obtained by RT-PCR from total RNAs extracted from HEK293T cells. The coding sequences for expression in human cell lines were constructed into pcDNA3.1(+) vector. The coding sequences for expression and coexpression in insect cells were constructed into pKL vector. The designed sgRNAs for *THUMPD2* (NM_025264.5) and *THUMPD3* were constructed into px330-mcherry vector. The coding sequences of mouse *Thumpd3* (NM_008188.3) and mouse *Trmt112* (NM_001166370.1) were amplified from cDNA, which was obtained by RT-PCR from total RNAs extracted from mouse tissues, and then, constructed into pMD™18-T vector (Takara Bio) and pcDNA3.1(+) vector, respectively; these two plasmids were used for standard curve in absolute quantification in real-time PCR.

Western blotting

Cell lysates, cell fraction extracts, and immunoprecipitation complexes were separated by sodium dodecyl sulfate-polyacrylamide gel electrophoresis (SDS-PAGE), and the protein bands were transferred to 0.2 μm PVDF membranes. After blocking with 5% (w/v) non-fat dried milk, the membranes with targeted proteins were incubated with the corresponding primary antibodies overnight at 4°C. Membranes were then washed three times with PBST (phosphate-buffered saline with Tween-20) and incubated with HRP-conjugated secondary antibody at room temperature for 60 min. After washing three times with PBST, the membranes were treated with the chemiluminescent substrates (EpiZyme), and imaging was performed using the Amersham Imager 680 (GE Healthcare).

Gene expression and protein purification

The gene encoding THUMPD3 fused with a C-terminal His_{10}-tag (THUMPD3-His) was expressed or co-expressed with TRMT112 in baculovirus-mediated transduction of High Five insect cells (47,48). 60 h post infection, the cells were harvested by centrifugation at 1000 g and frozen at -80°C until purification. After thawing, cells were lysed by sonication in buffer A containing 50 mM Tris–HCl (pH 7.5), 500 mM NaCl, 10% glycerol, 5 mM imidazole and 10 mM β-Me with 1 mM Phenylmethylsulfonyl Fluoride (PMSF). The supernatant was collected by centrifugation at 16 000 g at 4°C for 45 min and then loaded onto a Ni^{2+}-NTA Superflow column equilibrated with buffer A. After washing with two column volumes of buffer A supplemented with 1 M NaCl and with 25 mM imidazole, the proteins were eluted in buffer A supplemented with 400 mM imidazole. The eluted proteins were concentrated and then applied into Superdex 200 Increase 10/300 GL column (GE Healthcare) in a buffer B containing 50 mM Tris–HCl (pH 7.5) and 300 mM NaCl. The fractions were analysed

by SDS-PAGE and concentrated for the follow-up experiments.

Confocal immunofluorescence microscopy

HEK293T cells were transfected with pcDNA3.1(+)-THUMPD3-HA plasmid. After transfection for 24 h, the cells were fixed in 4% paraformaldehyde for 10 min and then permeated in 0.2% Triton X-100 for 5 min on ice. After washing with phosphate-buffered saline (PBS), the fixed cells were blocked in PBS containing 5% BSA and then incubated with rabbit anti-HA antibodies with 1:800 dilution overnight at 4°C. The cells were then immunolabeled with Alexa Fluor 488-conjugated goat anti-rabbit IgG in PBS with 1:100 dilution for 2 h and the nuclear counterstain DAPI for 5 min at room temperature. Fluorescent images were taken and analysed using an LSM980 Airyscan2 confocal microscope (Zeiss).

Subcellular fractionation

Separation of cytosol and nucleus extracts was performed in HeLa cells using low permeability buffer (20 mM Tris–HCl (pH 7.4), 10 mM NaCl, 3 mM $MgCl_2$ and 1× protease inhibitor cocktail (EDTA-free)) followed by addition of NP-40 at final concentration 5% and vortex for 10 sec. Centrifuge lysates at 3000 rpm for 10 min at 4°C. The supernatant contains cytosol fraction and the pellet is the nucleus fraction. The pellet was suspended in low permeability buffer and disrupted by Ultrasonic homogenizer (Scientz).

Immunoprecipitation

For immunoprecipitation, HEK293T cells were transfected with pcDNA3.1(+)-THUMPD3-HA or pcDNA3.1(+)-TRMT112-Flag. Lipofectamine 2000 was used for transfection according to the manufacturer's protocol. After transfection for 36 h, the cells were washed three times with ice-cold PBS and then lysed with 1 ml of ice-cold lysis buffer (50 mM Tris–HCl (pH 7.4), 150 mM NaCl, 1 mM EDTA, 1% NP-40, and 0.25% deoxycholic acid) supplemented with a Proteinase Inhibitor Cocktail (MedChemExpress). The supernatant was collected by centrifugation at 12 000 rpm for 20 min. Subsequently, the supernatant was incubated with the anti-HA magnetic beads or anti-Flag magnetic beads with gentle agitation for 6 h. Recovered immunoprecipitation complexes were washed three times with ice-cold lysis buffer. All procedures were performed at 4°C. The immunoprecipitation complexes were eluted by incubating with protein loading buffer (10 mM Tris–HCl (pH 6.8), 2% sodium dodecyl sulfate, 0.1% bromophenol blue, 10% glycerol and 100 mM dithiothreitol (DTT)).

Construction of knockout cell lines

Sense and anti-sense oligonucleotides for a guide RNA (sgRNA) were computationally designed for the selected genomic targets (http://crispor.tefor.net) and were cloned into pX330-mcherry vector (Addgene, 98750) which expresses red fluorescence protein (49). Two sgRNA sets were designed for *THUMPD2* and *THUMPD3*, respectively. The sgRNA sequences for relevant genes and targeting sites are shown in Figure 1. For generating KO cell lines, sgRNA plasmids were transfected in HEK293T cells using Lipofectamine 2000 as transfection reagent. After transfection for 36 h, HEK293T cells expressing red fluorescent protein were enriched by FACS Aria Fusion SORP (BD Bioscience) and plated into a dish at a very low density. After 7–14 days, single colonies were picked and plated into a well of a 96-well plate. Genotype of the stable cell lines was identified by sequencing single cloned PCR products based upon the following primers, and the target sites for PCR primers or the results for PCR products were shown in Supplementary Figure S1.

THUMPD2-identify-primer forward: GGTAATTGAG TTTGAGGGTGATGA

THUMPD2-identify- primer reverse: CCCATACCCA TAACAAAGCCACT

THUMPD3-identify- primer forward: CTCTGTGCCC ATGTTTATTCAACC

THUMPD3-identify- primer reverse: CACAAACTGT CACTTGTTCTTTGG

Isolation of cellular total tRNAs

Total RNAs from WT, *THUMPD2*-KO and *THUMPD3*-KO HEK293T cell lines were extracted using TRNzol Universal reagent. The total RNAs were separated by electrophoresis on 12% TBE–urea PAGE, and the tRNA bands (range from 70 to 90 nt) were excised and collected. Subsequently, the total tRNAs from the gel were extracted using 0.5 mM NaAc and precipitated with 70% (v/v) ethanol.

Isolation of endogenous specific tRNAs by biotinylated DNA probes

The endogenous specific tRNAs used in this study were isolated from total cellular RNAs by their own biotinylated DNA probes using Streptavidin agarose resin as described before (50). The biotinylated DNA probes were designed to complement about 30 nt of the tRNAs. According to the tRNA database (1,51), eight different tRNAs from mammals were sequenced with a m^2G6 modification. Thus, we designed eight DNA probes for isolating each of the eight kinds of tRNAs, respectively, including $tRNA^{Gly}$(GCC), $tRNA^{Gly}$(CCC)-1, $tRNA^{Gly}$(CCC)-2, $tRNA^{Leu}$(CAG), $tRNA^{Leu}$(CAA), $tRNA^{Lys}$(CUU), $tRNA^{Tyr}$(GUA) and $tRNA^{Met}$(CAU). 30 μl of high-capacity streptavidin-conjugated agarose beads were first washed with 10 mM Tris–HCl (pH 7.5) and then resuspended in 100 mM Tris–HCl (pH 7.5). Subsequently, 200 μM biotinylated oligonucleotides probes were mixed with beads and incubated at room temperature for 90 min. After the incubation, the oligonucleotide-conjugated beads were then washed three times with 10 mM Tris–HCl (pH 7.5). The total RNAs were dissolved in 6× NTE solution (20 × NTE solution is 4 M NaCl, 0.4 M Tris–HCl (pH 7.5), and 50 mM EDTA). The oligonucleotide-conjugated beads and total RNAs were mixed together and heated at 70°C for 30 min and subsequently cooled down slowly to 30°C. Then, the beads were washed with 3× NTE for once and 1× NTE for twice. The specific tRNA retained on the

beads was eluted with 0.1× NTE at 70°C and precipitated using 70% (v/v) ethanol. The eight kinds of tRNAs and their probes for tRNA isolation used in this study are shown as follows.

For hctRNA^{Gly}(CCC)-1:
5′Biotin-TTGGCCGGGAATTGAACCCGGGTCTCCCGCGTGGGA
For hctRNA^{Gly}(CCC)-2:
5′Biotin-TCTTGCATGATACCACTACACCAGCGGCGC
For hctRNA^{Gly}(GCC):
5′Biotin-GCGAGAATTCTACCACTGAACCACCCATGC
For hctRNA^{Leu}(CAG):
5′Biotin-CAGCGCCTTAGACCGCTCGGCCATCCTGAC
For hctRNA^{Leu}(CAA):
5′Biotin-TGGCGCCTTAGACCACTCGGCCATCCTGAC
For hctRNA^{Lys}(CUU):
5′Biotin-CCCATGCTCTACCGACTGAGCTAGCCGGGC
For hctRNA^{Tyr}(GUA):
5′Biotin- CTAAGGATCTACAGTCCTCCGCTCTACCAGCT
For hctRNA^{Met}(CAU):
5′Biotin-CTGACGCGCTACCTACTGCGCTAACGAGGC

Relative quantitative analysis of tRNA modifications using UPLC-MS/MS

200 ng of specific endogenous tRNAs isolated by the biotinylated DNA probes or tRNA transcripts were hydrolysed with 0.2 μl benzonase, 0.25 μl phosphodiesterase I, and 0.25 μl bacterial alkaline phosphatase in a 20 μl solution including 4 mM NH_4OAc at 37°C overnight. After complete hydrolysis, the products were dissolved in acetonitrile and then applied to ultra-performance liquid chromatography-mass spectrometry/mass spectrometry (UPLC-MS/MS). The nucleosides were separated on a Hilic column (Atlantis® HILIC Silica 3 μm, 2.1 × 150 mm Column) and then detected by a triple quadrupole mass spectrometer (AB Sciex QTRAP 6500+) in the positive ion multiple reaction monitoring (MRM) mode. The nucleosides were quantified using the nucleoside-to-base ion mass transitions of 268.1–136.2 (A), 298.1–166.1 (m^2G) and 321.1–180.2 ($m^2{}_2G$). Quantification was performed by comparison with the standard curve obtained from pure nucleoside standards running in the same batch.

LC–ESI-MS for RNA fragment analysis

20 pmol modified or unmodified tRNAs were incubated at 37°C for 1 h in a digestion mixture containing 25 mM NH_4OAc and dialyzed RNase T1 (2 U/μl, Thermo Fisher Scientific). The digested products were dissolved in an equal volume of 0.1 M triethylamine acetate (TEAA) (pH 7.0) and then applied to LC–ESI-MS on a Q Exactive Orbitrap mass spectrometer (Thermo Fisher Scientific). Resulting tRNA fragments were separated at a 0.2 ml/min flow rate by an OST C18 column (Waters, 1.7 μm, 2.1 × 150 mm). The mobile phase consisted of ultra-pure water containing 0.1 M 1,1,1,3,3,3-hexafluoro-2-propanol (HFIP) (pH 7.0), 15 mM triethylamine (TEA) (solvent A) and methanol containing 0.1 mM HFIP, 15 mM TEA (solvent B). The column was equilibrated in 1% B, and the gradient program was as follows: 0–2 min, 1% B; 2–30 min, 1–25% B; 30-35 min, 25–95% B; 35–40 min, 95% B; 40–40.1 min, 95–1% B and 40.1–50 min, 1% B. Column temperature was maintained at 60°C. The eluent was ionized by an ESI source in negative polarity mode and scanned over an m/z range of 405–2000. Ion source parameters were optimized by oligonucleotide standards ranging from 15 to 30 nt. Thermo Xcalibur Qual Browser extracted signals of modified or unmodified tRNA fragments. The sequence and modification sites of each fragment were confirmed by MS1 and HCD MS2 spectra.

Preparation of transcript tRNAs

The DNA sequences of the T7 promoter and the tRNAs (tRNA^{Gly}(GCC)-1, tRNA^{Gly}(GCC)-2, tRNA^{Gly}(CCC)-1 and tRNA^{Gly}(CCC)-2; tRNA^{Asp}(GUC)-2; tRNA^{Glu}(CUC)-1; tRNA^{His}(GUG)-1; tRNA^{Ile}(AAU)-2 and tRNA^{Ile}(GAU)-1; tRNA^{Leu}(UAA)-3, tRNA^{Leu}(CAA)-1 and tRNA^{Leu}(CAG)-1; tRNA^{Lys}(CUU)-1 and tRNA^{Lys}(UUU)-1; tRNA^{Pro}(AGG)-2, tRNA^{Pro}(CGG)-1 and tRNA^{Pro}(UGG)-1; tRNA^{Phe}(GAA)-3, tRNA^{Met}(CAU)-1, tRNA^{Glu}(UUC)-3, tRNA^{Leu}(UAA)-2, tRNA^{Arg}(CCU)-3, tRNA^{Thr}(CGU)-2, tRNA^{Ser}(GCU)-1, tRNA^{Ser}(UGA)-1 and tRNA^{Ser}(CGA)-1; tRNA^{Tyr}(GUA)-1; tRNA^{Met}(CAU)-2; tRNA^{Trp}(CCA)-2) were obtained from the GtRNAdb database (51) and cloned into pTrc99b vector (two restriction enzyme cutting sites for the vector were EcoRI and BamHI) to construct pTrc99b-T7-tRNA plasmids. The sequences of mutated tRNAs including tRNA^{Leu}(CAG)-1-Mut, tRNA^{Leu}(CAG)-1-Δ3′-CCA, 5′-tRF-tRNA^{Gly}(GCC), and mini-helix-tRNA^{Gly}(GCC) were constructed into pTrc99b vector as well as wildtype tRNAs. All tRNA transcripts were generated via *in vitro* transcription using T7 RNA polymerase, as described previously (52). The transcribed tRNAs were denatured and annealed to form the right conformation in 5 mM magnesium chloride ($MgCl_2$). Subsequently, the concentration of tRNAs was determined by UV absorbance at 260 nm, and the molar absorption coefficient was calculated based on the sequence of each tRNA (53).

Isothermal titration calorimetry assays

Isothermal titration calorimetry (ITC) measurements were performed at 25°C, using MicroCal PEAQ-ITC (Malvern Panalytical) or Isothermal titration microcalorimetry ITC-200 (Malvern Instruments). Experiments were performed by titration of 20 injections of 2 μl of sinefungin (SFG) (1 mM) into the Sample Cell containing around 50 μM purified THUMPD3 or THUMPD3–TRMT112 protein solution. The SFG and corresponding protein were hold in the same buffer C (50 mM Tris–HCl (pH 7.5), 300 mM NaCl). Titration of SFG to the same buffer was used as control to evaluated whether the titration system was normal or not.

Binding isotherms were fitted by non-linear regression using MicroCal PEAQ-ITC analysis software or Origin Software version 7.0 (MicroCal). The ITC data were fitted to a one-site binding model using the two software as described as upon.

Electrophoretic mobility shift assays (EMSAs)

Purified THUMPD3 (final concentrations, 0.1, 0.2, 0.4, 0.6, 0.8, 1.0 and 2.0 μM) or THUMPD3–TRMT112 (final concentrations, 0.1, 0.2, 0.4, 0.6, 0.8, 1.0, 2.0 and 4.0 μM) in buffer C and $tRNA^{Leu}$(CAG)-1 or $tRNA^{Leu}$(CAG)-1-Δ3′-CCA transcripts (final concentration was 200 nM) in 5 mM $MgCl_2$ were incubated in 20 μl reaction system at 4°C for 20 min. After incubation, 4 μl of RNA loading solution (60% glycerol, 30 mM EDTA, pH 8.0, 0.05% bromophenol blue, and 0.05% Xylene Cyanol FF) was added into each sample and loaded immediately onto a 6% polyacrylamide native gel. Electrophoresis was carried out at 4°C at a constant voltage of 120 V for 80 min, using 50 mM Tris-glycine buffer. The gel was stained with GelStain (TransGen Biotech) for detection of RNA. The RNA bands were quantified by using a Gel Dox XR + imaging system (Bio-Rad).

Cell counting kit-8 (CCK-8) assays

Cell proliferation was determined using the Cell Counting Kit-8. Briefly, 1.5×10^3 WT or *THUMPD3* knockout HEK293T cell lines were seeded in a 96-well flat-bottomed plate under normal culture. At days 1, 2, 3, 4 and 5, 10 μl of CCK-8 reagent was added into each well and the cells were incubated for 2 h at 37°C with 5% CO_2. The optical density at 450 nm (OD450) was measured using a Spark multimode plate reader (Tecan). The experiments were repeated for three times and assayed the growth curve as above.

Measurement of tRNA methyltransferase activity *in vitro*

Assays for methyltransferase activity of purified THUMPD3 or THUMPD3–TRMT112 using ^{3}H-isotope were conducted as follows: 0.5 μM protein, 5 μM tRNA, and 200 μM [Methyl-^{3}H] SAM in buffer D (50 mM Tris–HCl (pH 7.5), 100 mM NaCl, 5 mM $MgCl_2$, and 2 mM DTT). Reaction mixtures were incubated for various time intervals at 37°C and then aliquots were spotted on filters and quenched by 5% trichloroacetic acid. The amount of radioactive [^{3}H]-methyl-tRNA was measured using a Beckman Ls6500 scintillation counting apparatus.

To confirm the modification introduced on tRNAs by purified THUMPD3–TRMT112 is indeed m^2G, the reactions were carried out at 37°C for 2 h in a 50 μl reaction mixture containing 50 mM Tris–HCl (pH 7.5), 100 mM NaCl, 5 mM $MgCl_2$, 2 mM DTT, 200 μM SAM, 5 μM tRNA, and 0.5 μM THUMPD3 or 1 μM THUMPD3–TRMT112, respectively. After reaction, the tRNAs were extracted with phenol/chloroform and precipitated using a two-fold volume of ethanol. Subsequently, the tRNAs were digested with benzonase, phosphodiesterase I, and bacterial alkaline phosphatase and then subjected to UPLC-MS/MS analysis to detect and quantify m^2G as described above.

Polysome profiling

Polysome profiling was performed as described with some modifications (54). Cells were incubated for 5 min at 37°C in medium supplemented with 100 μg/ml CHX. Resuspend cells in 425 μl hypotonic buffer (5 mM Tris–HCl (pH 7.5), 2.5 mM $MgCl_2$, 1.5 mM KCl and 1× protease inhibitor cocktail (EDTA-free)) added with 100 units of RNase inhibitor, 5 μl 10 mg/ml CHX, and 1 μl 1 M DTT, and vortex for 5 sec followed by addition of 25 μl of 10% Triton X-100 and 25 μl of 10% Sodium deoxycholate and vortex for 5 s. Centrifuge lysates at 16 000 g for 7 min at 4°C and transfer the cytosolic and endoplasmic reticulum-associated ribosomes to a new tube. The ribosomes were layered onto a linear sucrose gradient (10–50%) sucrose (Thermo Fisher) (w/v) and centrifuged in a SW41Ti rotor (Beckman) at 36 000 rpm for 2 h at 4°C. Polysome profiles were generated using a BioComp Gradient Station (BioComp).

Absolute quantitative real-time PCR (qRT-PCR)

Total RNAs from mouse tissues were extracted using TRNzol Universal Reagent according to the manufacturer's instructions. The first-strand DNA synthesis using total RNAs from mouse tissues as the templates was performed with HiScript III RT SuperMix for QPCR (+gDNA wiper). The standard material for calibration curves of coding sequence of mouse *Thumpd3* and *Trmt112* were constructed into plasmids pMD™18-T-THUMPD3 and pcDNA3.1(+)-TRMT112, respectively. The copy number of standards could range from 10^1 to 10^{10}, which based on the known concentrations of DNA standard molecules. qRT-PCR was performed using the standard curve method in QuantStudio 7 (Life Technology) with ChamQ Universal SYBR QPCR Master Mix as the dsDNA fluorescence dye. The reactions were performed under the following conditions: 95°C for 2 min; 40 cycles of 95°C for 10 s, 55°C for 30 s, 72°C for 30 s. The amplification efficiency (E%) of standard material must in the range of 90–110%. Thus, we designed several primers for each gene and pick up the one that meets the amplification efficiency. The primers finally used for the *Thumpd3* and *Trmt112* in the qRT-PCR are listed as follow.

Mouse- *Thumpd3*-primer forward:
GCCTGGGTATGAACCTTGATG
Mouse- *Thumpd3*-primer reverse:
GCCAGACTTTCCACTGCAATATC
Mouse- *Trmt112*-primer forward:
GAGCACGACGAGACATTTTTGA
Mouse- *Trmt112*-primer reverse:
GGTGCCCTCCAGTACATCA

RESULTS

Knocking out of *THUMPD3* decreased the m^2G level of total tRNA in human cells

To identify the enzymes responsible for m^2G at the sixth position of eukaryotic tRNAs, we used a reverse genetics approach coupled with RNA-mass spectrometry (RNA-MS). First, we chose those previously uncharacterized MTase genes that are not conserved in fungi, because m^2G is not present in fungi. Among them, we fo-

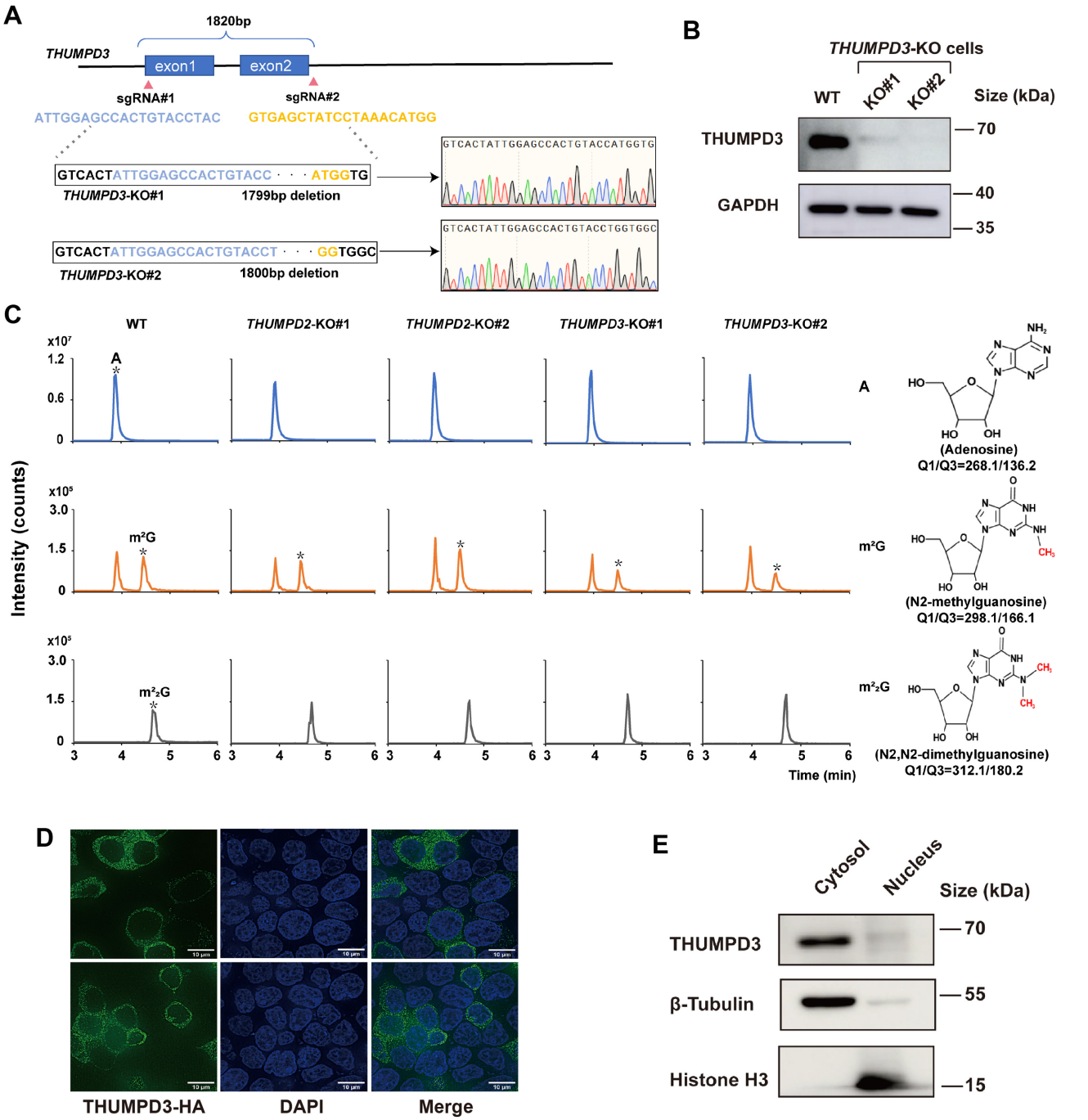

Figure 1. Analysis of m^2G and $m^2{}_2G$ modifications of total tRNAs from *THUMPD2*$^{-/-}$ and *THUMPD3*$^{-/-}$ HEK293T cells. (**A**) Genetic analysis of the human *THUMPD3* genes and target sites of deletions introduced by the CRISPR-Cas9 system. The target sequence of sgRNAs are listed, and the resulting mutated sequences are boxed. Sequences of both alleles in KO#1 and KO#2 HEK293T cell lines are aligned. (**B**) Western blotting analysis showing the absence of THUMPD3 in KO cells. (**C**) Mass chromatograms of nucleosides, A (Q1/Q3 = 268.1/136.2) (top), m^2G (Q1/Q3 = 298.1/166.1) (middle), and $m^2{}_2G$ (Q1/Q3 = 321.1/180.2) (bottom) of total tRNAs extracted from WT, *THUMPD2*-KO#1, *THUMPD2*-KO#2, *THUMPD3*-KO#1, and *THUMPD3*-KO#2 HEK293T cell lines. Target peaks are indicated by a black asterisk. The relative abundance of A was used as control. A, adenosine; m^2G, N2-methylguanosine; $m^2{}_2G$, N2, N2-dimethylguanosine. Q1/Q3: the mass of the precursor ion and the mass of the product ion. (**D**) Immunofluorescence labeling of THUMPD3-HA (green) in HEK293T cells. The nucleus was stained using DAPI (blue). Scale bar, 10 μm. (**E**) Subcellular localization of endogenous THUMPD3 analyzed by subcellular fractionation assays. Cytosol and nucleus fractions were separated from HeLa cells. β-Tubulin and Histone H3 were used as indicators of the cytosol and nucleus fractions, respectively.

cused on THUMPD2 (THUMP domain-containing protein 2) and THUMPD3 because they both have a predicted domain architecture similar to some other known tRNA:m^2G MTases such as *Pf*Trm14, *Tt*TrmN and Trm11. We therefore knocked out *THUMPD2* and *THUMPD3* genes respectively in HEK293T cells using the CRISPR-Cas9 system. Four knockout (KO) cell lines were obtained and confirmed by sequencing, two of which had deletion-mediated frameshift mutations in *THUMPD2* (Supplementary Figure S1A), and the other two had deletion-mediated frameshift mutations in *THUMPD3* (Figure 1A). The deletion fragments of *THUMPD2* and *THUMPD3* were further verified using PCR (Supplementary Figure S1B–D). Moreover, the absence of the protein expression of THUMPD3 was further identified using western blotting analysis (Figure 1B). Total tRNAs were isolated from *THUMPD2*-KO#1, *THUMPD2*-KO#2, *THUMPD3*-KO#1, *THUMPD3*-KO#2, and wild-type (WT) cells and then subjected to RNA-MS (Figure 1C). Notably, the level of m^2G was significantly decreased in *THUMPD3*-KO#1 and *THUMPD3*-KO#2 and was about half the level of m^2G present in the WT; however, no detectable change was observed in *THUMPD2*-KO#1 or *THUMPD2*-KO#2. Interestingly, the level of $m^2{}_2G$ did not change in any of the cell lines. These results suggested that THUMPD3, but not THUMPD2, contributes to the m^2G modification of total tRNAs.

The subcellular localization of THUMPD3 was further detected. We first expressed HA-tagged THUMPD3 (THUMPD3-HA) in HEK293T cells. Protein immunofluorescence labeling assays showed that THUMPD3-HA was predominantly located in the cytoplasm (Figure 1D). The subcellular localization of endogenous THUMPD3 was further checked by cytosol/nuclear fractionation assays, and western blotting analysis showed that almost all THUMPD3 was located in the cytosol fraction of HeLa cells (Figure 1E).

THUMPD3 is responsible for the tRNA:m^2G6 modification *in vivo*

To further verify whether the THUMPD3 is responsible for m^2G at the sixth position of tRNAs, we searched the modification database (https://iimcb.genesilico.pl/modomics/) and found that at least eight species of tRNAs contain m^2G6 in mammals, and all them are cytoplasmic tRNAs (1). To identify whether all of them were the substrates of THUMPD3 in human cells, we used biotin-labeled DNA probes that were complementary to specific tRNAs to purify those endogenous tRNAs in *THUMPD3* KO and WT cell lines, respectively. The purified tRNAs were subsequently digested and subjected to RNA-MS (Figure 2A). Notably, the m^2G level decreased in all eight tRNAs when *THUMPD3* was knocked out (Figure 2B and C). In the first group, m^2G is only present at the sixth position of tRNAs including $tRNA^{Gly}$(CCC)-1, $tRNA^{Gly}$(CCC)-2, and $tRNA^{Gly}$(GCC), and the level of m^2G in these tRNAs became undetectable in both *THUMPD3* KO cell lines (Figure 2B), indicating the important role of THUMPD3 for m^2G modification of these tRNAs, and suggesting that THUMPD3 modifies the sixth position in those tRNAs. In the second group, m^2G was present at both the 6^{th} and 10^{th} positions of tRNAs, including $tRNA^{Leu}$(CAG), $tRNA^{Leu}$(CAA), $tRNA^{Lys}$(CUU), $tRNA^{Tyr}$(GUA) and $tRNA^{Met}$(CAU). The level of m^2G in these tRNAs was also dramatically decreased in both *THUMPD3* KO cell lines when compared with those in the WT (Figure 2C) suggesting these five tRNAs were also the substrates of THUMPD3. The above results using purified endogenous tRNAs strongly suggested that THUMPD3 is a tRNA m^2G6-methyltransferase at least for eight tRNAs tested.

THUMPD3 alone is enzymatically inactive *in vitro*

*Tt*TrmN and its ortholog protein Trm14 from archaea were reported to work alone to methylate guanosine at the sixth position (m^2G6) of tRNAs *in vitro* (33,44). Therefore, to verify the enzymatic activity of THUMPD3 *in vitro*, the coding sequence of human *THUMPD3* was constructed and expressed in an insect cell expression system. THUMPD3 was produced as a soluble protein and could be purified following two-step chromatography (Figure 3A and B). Full length THUMPD3 contains 507 amino acids (aa) and its theoretical molecular weight is 57 kDa. However, gel filtration chromatogram analysis showed that purified THUMPD3 was eluted in the fractions larger than 660 kDa in Superdex 200 Increase 10/300 GL column (Figure 3A), suggesting that THUMPD3 is highly polymerized *in vitro*. The tRNA methylation activity of purified THUMPD3 was then tested by measuring the transfer of [methyl-^{3}H] from SAM onto several tRNA transcripts, including $tRNA^{Gly}$(GCC)-2, $tRNA^{Gly}$(CCC)-2, $tRNA^{Leu}$(CAA)-1, $tRNA^{Tyr}$(GUA)-1, and $tRNA^{Met}$(CAU)-2, representing four tRNAs that contain G at the sixth position plus $tRNA^{Met}$(CAU)-2, which does not (Figure 3C). The results showed that THUMPD3 was completely inactive. The *in vitro* activity of THUMPD3 was further analyzed using RNA-MS (Figure 3D); however, no detectable m^2G was found in any of the five tRNAs after an incubation with THUMPD3 and SAM. We then analyzed the binding affinity of THUMPD3 for $tRNA^{Leu}$(CAG)-1 using EMSAs (Figure 3E), and found that THUMPD3 alone could not bind the substrate tRNA *in vitro*. Next, we performed ITC to measure the SAM-binding capability of THUMPD3 by titration of a SAM analog (sinefungin, SFG) to THUMPD3 (Figure 3F). The results indicated that THUMPD3 alone could not bind SAM *in vitro*.

Together, these results showed that standalone THUMPD3 is unable to bind with tRNA or SAM, and is enzymatically inactive as a tRNA methyltransferase *in vitro*.

The methyltransferase activator TRMT112 interacts with THUMPD3 *in vivo* and *in vitro*

In eukaryotes, many RNA modification enzymes consisting of a catalytic subunit, such as FTSJ1 (55), Trm61 (56) and Trm11 (34), have been shown to work as a complex with distinct auxiliary proteins for their tRNA modifications (57). Therefore, we hypothesized that auxiliary factors might work with THUMPD3 to exert tRNA

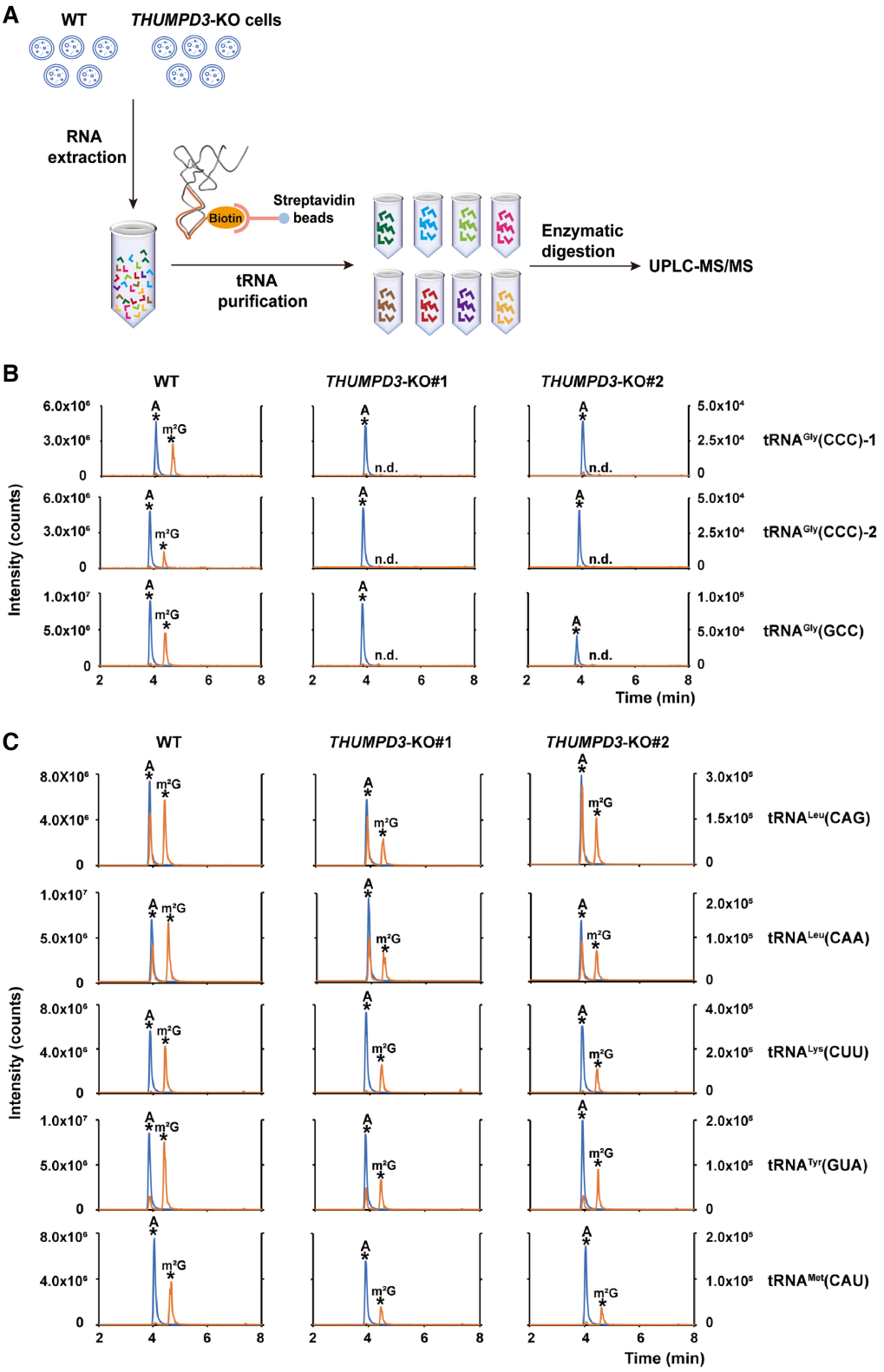

Figure 2. Identification of the tRNA substrates profile of THUMPD3 in HEK293T cells. (**A**) Schematic diagram illustrating the principle of specific tRNAs purified from WT and *THUMPD3* KO#1 and #2 HEK293T cell lines by the binding affinity of biotin-DNA probes and streptavidin-conjugated agarose beads. (**B**) Mass chromatograms of A and m^2G of $tRNA^{Gly}$(CCC)-1, $tRNA^{Gly}$(CCC)-2, and $tRNA^{Gly}$(GCC) purified from WT (left), *THUMPD3*-KO#1 (middle), and *THUMPD3*-KO#2 (right) HEK293T cell lines. Target peaks are indicated by black asterisks. n.d., not detectable. **(C)** Mass chromatograms of A and m^2G of $tRNA^{Leu}$(CAG), $tRNA^{Leu}$(CAA), $tRNA^{Lys}$(CUU), $tRNA^{Tyr}$(GUA), and $tRNA^{Met}$(CAU) purified from WT (left), *THUMPD3*-KO#1 (middle), and *THUMPD3*-KO#2 (right) HEK293T cell lines. Target peaks are indicated by black asterisks. In B and C, the value of left vertical axis stands for the intensity of A and the value of right vertical axis stands for the intensity of m^2G.

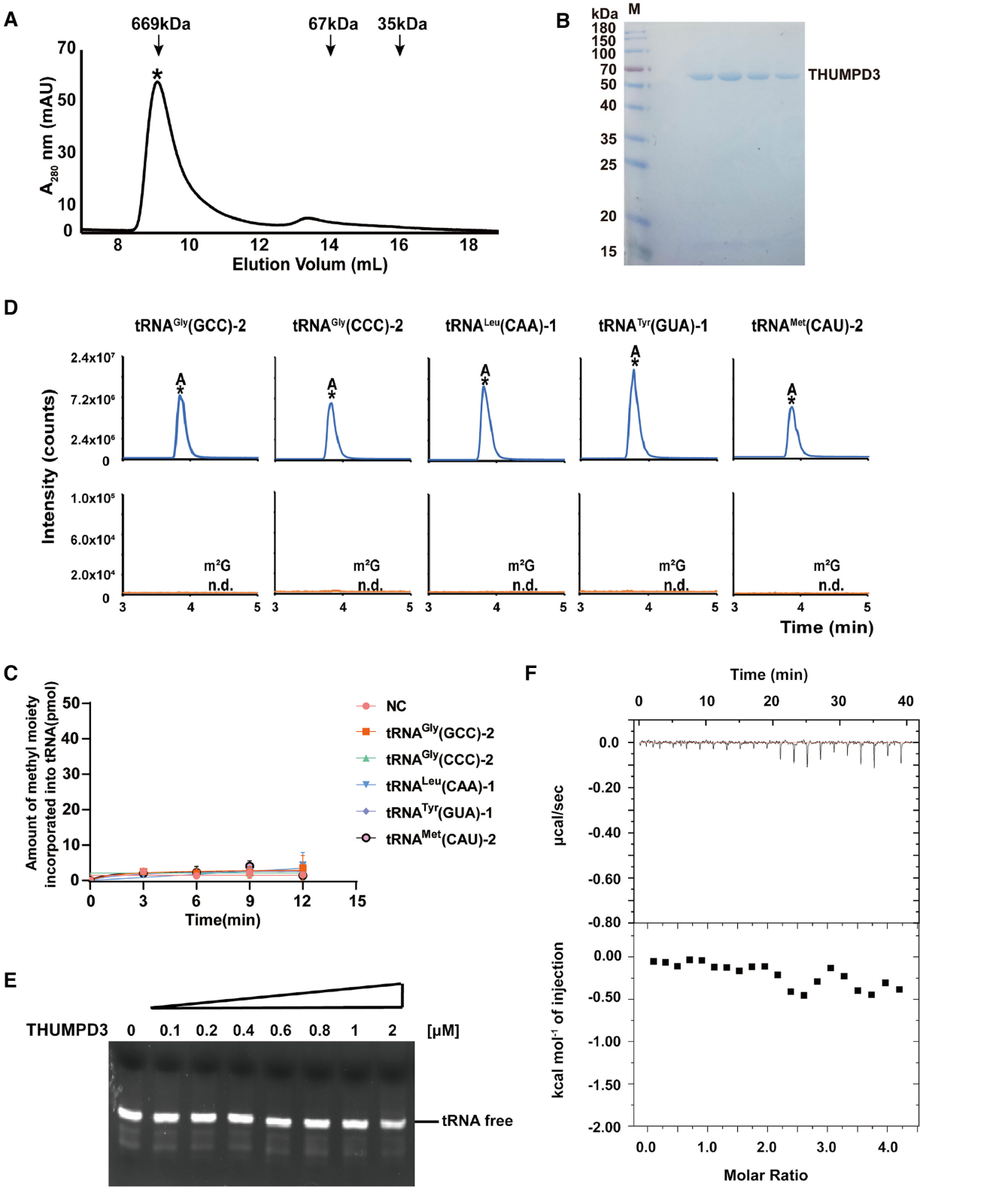

Figure 3. Standalone THUMPD3 is enzymatically inactive *in vitro*. (**A**) Gel filtration chromatogram of THUMPD3 on Superdex 200 Increase 10/300 GL column, the standard molecular weight is marked on the top. The THUMPD3 peak is indicated by a black asterisk. (**B**) Electrophoresis analysis of purified THUMPD3 on 12% SDS-PAGE. (**C**) The methyltransferase activity assays of purified THUMPD3 toward $tRNA^{Gly}$(GCC)-2, $tRNA^{Gly}$(CCC)-2, $tRNA^{Leu}$(CAA)-1, $tRNA^{Tyr}$(GUA)-1 and $tRNA^{Met}$(CAU)-2. (**D**) Mass chromatograms of A and m^2G of $tRNA^{Gly}$(GCC)-2, $tRNA^{Gly}$(CCC)-2, $tRNA^{Leu}$(CAA)-1, $tRNA^{Tyr}$(GUA)-1, and $tRNA^{Met}$(CAU)-2 after incubation with THUMPD3 in the presence of SAM. Target peaks are indicated by black asterisks. n.d., not detectable. (**E**) The binding affinity of purified THUMPD3 for $tRNA^{Leu}$(CAG)-1 analyzed by the EMSAs. For the reaction, different concentrations of THUMPD3 and 200 nM $tRNA^{Leu}$(CAG)-1 transcripts were incubated. (**F**) Measuring the binding affinity of THUMPD3 to sinefungin (a SAM analog, SFG) using ITC.

methylation. We performed immunoprecipitation followed by mass-spectrometry (IP-MS) for THUMPD3 to identify its interaction proteins. THUMPD3-HA was overexpressed in *THUMPD3*-KO#1 cell and pulled down using anti-HA magnetic beads (Figure 4A), and the IP-MS results showed that a known methyltransferase activator, TRMT112, which has been reported to participate in the methylation process of rRNAs, tRNAs, and proteins with various methyltransferases, was top of the list of THUMPD3-interacting proteins (Figure 4B, Supplementary Table S1). Human TRMT112 contains 125 aa and its theoretical molecular weight is about 14 kDa. The pull-down products of THUMPD3 were also analyzed by SDS-PAGE and sliver staining, besides THUMPD3 itself, an additional band (∼15 kDa) could be observed clearly compared with that of the control group (Figure 4C). This band was excised and subsequently identified by mass spectrometry as human TRMT112 (Figure 4D and E). One of the characteristic peptides of TRMT112 from IP-MS is shown in detail (Figure 4D), and all the peptides of TRMT112 that were identified by THUMPD3 IP-MS are marked on the primary sequence of TRMT112 (Figure 4E). These IP-MS results strongly suggested that THUMPD3 interacts with TRMT112 *in vivo*. We further used bidirectional immunoprecipitation to confirm the interaction between THUMPD3 and TRMT112 in HEK293T cells (Figure 4F and G).

Furthermore, to investigate whether the interaction between THUMPD3 and TRMT112 is direct, we performed *in vitro* co-expression and purification of these two proteins. The coding sequence of *THUMPD3* (with a 10× His-tag) and *TRMT112* (without any tag) were constructed into an insect cell expressing pKL-vector (Figure 4H). We found that TRMT112 could be co-purified with THUMPD3-10 × His on a Ni-affinity column, and the THUMPD3–TRMT112 complex was stable *in vitro* and could be eluted together using gel filtration chromatography (Figure 4I and J). Interestingly, when co-purified with TRMT112, THUMPD3 was no longer highly polymerized (Figure 4I). These results showed that THUMPD3 could interact strongly and directly with TRMT112 *in vivo* and *in vitro*.

The THUMPD3–TRMT112 complex robustly catalyzes the tRNA:m^{2}G6 modification *in vitro*

To further investigate whether the THUMPD3–TRMT112 complex could methylate tRNAs, the purified complex and the tRNA^{Leu}(CAG)-1 transcripts were used for methylation assays. First, we performed ITC to measure the SAM-binding capability of the THUMPD3–TRMT112 complex, which showed that SFG could bind to THUMPD3–TRMT112 with a dissociation constant (K_D) of about 12 μM (Figure 5A). Meanwhile, we analyzed the binding affinity of the THUMPD3–TRMT112 complex for tRNA^{Leu}(CAG)-1 using EMSAs (Figure 5B), and observed shifted tRNA bands after adding of 0.1 μM protein complex, and all the tRNAs were shifted in the presence of 4 μM protein complex. Taken together, these results showed that in contrast to standalone THUMPD3, the THUMPD3–TRMT112 complex could bind to SAM and tRNA efficiently. We then identified that the THUMPD3–TRMT112 complex showed robust methyl-transfer activity from SAM to tRNA^{Leu}(CAG)-1 *in vitro* (Figure 5C and D). RNA-MS was used to identify the modification type catalyzed by the THUMPD3–TRMT112 complex. One peak was detected after the reaction of tRNA^{Leu}(CAG)-1 with the THUMPD3–TRMT112 complex that accurately matched the m^{2}G standard (Figure 5C). To further confirm that the m^{2}G modification occurred at the 6th position, the G6-C67 base pair was mutated into C6-G67 in tRNA^{Leu}(CAG)-1 (tRNA^{Leu}(CAG)-1-Mut). We observed that tRNA^{Leu}(CAG)-1-Mut could not be methylated by the THUMPD3–TRMT112 complex (Figure 5C and D). These results indicated that the m^{2}G modification in tRNA^{Leu}(CAG)-1 introduced by the THUMPD3–TRMT112 complex was indeed at the sixth position.

The above results revealed that THUMPD3–TRMT112 is a bona fide RNA:m^{2}G methyltransferase working at the sixth position of tRNA *in vitro*.

THUMPD3–TRMT112 could catalyze m^{2}G modification in all the 26 tested G6-containing human cytoplasmic tRNAs

To identify the substrate specificity of the THUMPD3–TRMT112 complex, we screened its tRNA substrates *in vitro*. Besides tRNA^{Leu}(CAG)-1, we transcribed another 25 human cytoplasmic tRNA species that carry a G at position 6 (1,32), and incubated these tRNAs with the THUMPD3–TRMT112 complex and SAM. Combined with RNA-MS, we observed that the THUMPD3–TRMT112 complex could catalyze m^{2}G formation on all these tRNAs (tRNA^{Gly}(GCC)-2, tRNA^{Gly}(CCC)-2, tRNA^{Leu}(CAA)-1, tRNA^{Tyr}(GUA)-1, tRNA^{Gly}(GCC)-1, tRNA^{Gly}(CCC)-1, tRNA^{Asp}(GUC)-2, tRNA^{Glu}(CUC)-1, tRNA^{His}(GUG)-1, tRNA^{Ile}(AAU)-2, tRNA^{Ile}(GAU)-1, tRNA^{Lys}(CUU)-1, tRNA^{Lys}(UUU)-1, tRNA^{Pro}(AGG)-2, tRNA^{Pro}(CGG)-1, tRNA^{Pro}(UGG)-1, tRNA^{Phe}(GAA)-3, tRNA^{Met}(CAU)-1, tRNA^{Glu}(UUC)-3, tRNA^{Leu}(UAA)-2, tRNA^{Arg}(CCU)-3, tRNA^{Thr}(CGU)-2, tRNA^{Ser}(GCU)-1, tRNA^{Ser}(UGA)-1 and tRNA^{Ser}(CGA)-1) (Figure 6A and B, Supplementary Figure S2). These 26 tested tRNAs almost covered all the human cytoplasmic G6-containing tRNA species except for a few tRNA isodecoders that share high sequence similarity with the tested ones. To further verify that the m^{2}G was indeed added at the sixth position, we applied LC-ESI-MS (58) to analyze RNA fragments of tRNA^{Gly}(CCC)-1 and tRNA^{Asp}(GUC)-2 digested by RNase T1 (Figure 6C). RNA fragments containing m^{2}G6 nucleosides ('CAUUGp' and 'CAUUm^{2}Gp' of tRNA^{Gly}(CCC)-1; 'UCCUCGp' and 'UCCUCm^{2}Gp' of tRNA^{Asp}(GUC)-2) can be distinguished based on the difference between the observed mass and calculated m/z value, and the results showed that m^{2}G introduced by THUMPD3–TRMT112 was indeed occurred at the sixth position of tRNAs. In contrast, two cytoplasmic tRNAs, tRNA^{Met}(CAU)-2 and tRNA^{Leu}(UAA)-3, which do not carry G at their sixth position, could not be modified by the THUMPD3–TRMT112 complex, i.e. no detectable level of m^{2}G was found in these two tRNAs after incubation coupled with RNA-MS (Figure 6D). From all the sequenced tRNAs, bovine tRNA^{Trp}(CCA) exclusively

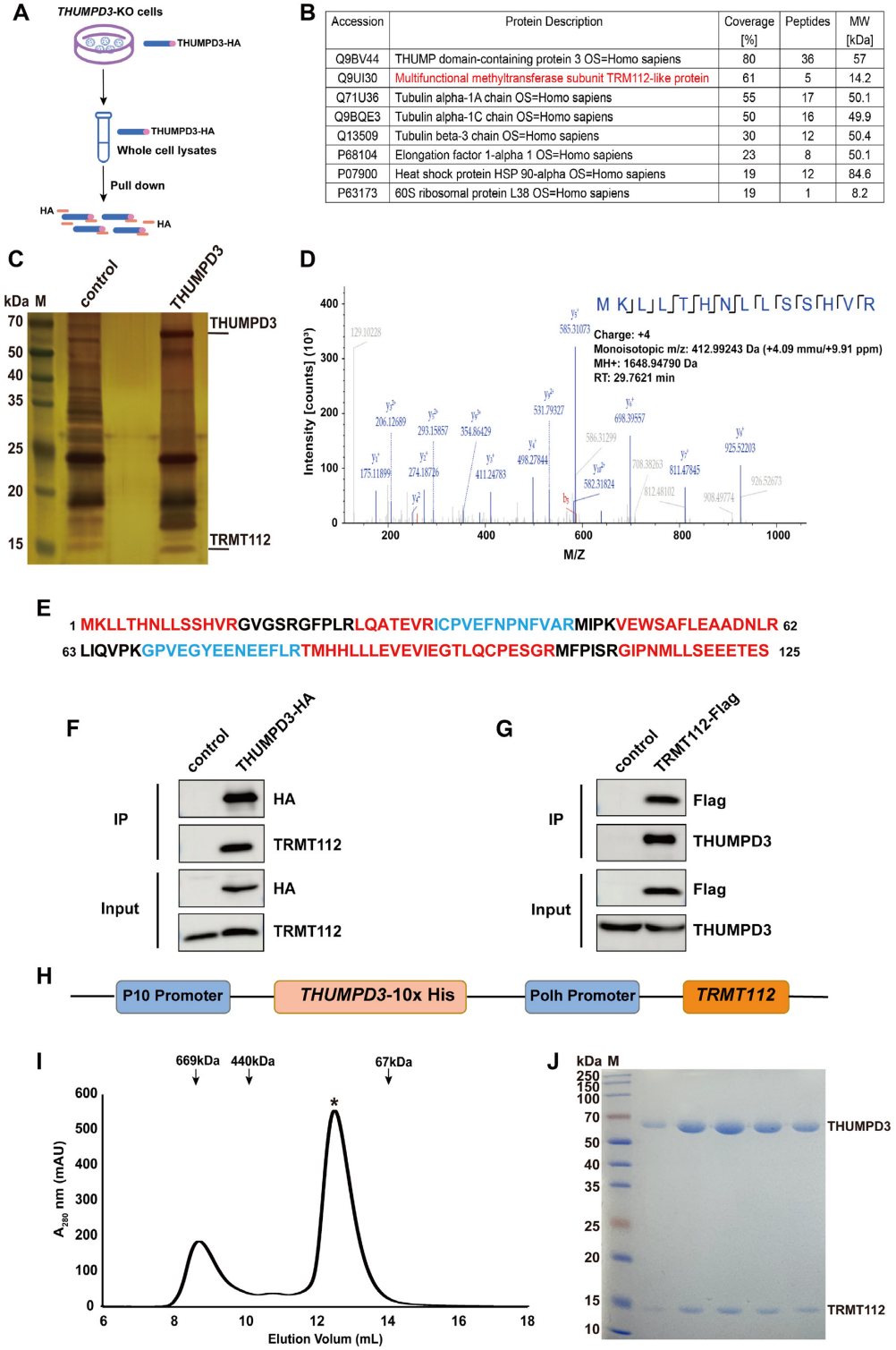

Accession	Protein Description	Coverage [%]	Peptides	MW [kDa]
Q9BV44	THUMP domain-containing protein 3 OS=Homo sapiens	80	36	57
Q9UI30	Multifunctional methyltransferase subunit TRM112-like protein	61	5	14.2
Q71U36	Tubulin alpha-1A chain OS=Homo sapiens	55	17	50.1
Q9BQE3	Tubulin alpha-1C chain OS=Homo sapiens	50	16	49.9
Q13509	Tubulin beta-3 chain OS=Homo sapiens	30	12	50.4
P68104	Elongation factor 1-alpha 1 OS=Homo sapiens	23	8	50.1
P07900	Heat shock protein HSP 90-alpha OS=Homo sapiens	19	12	84.6
P63173	60S ribosomal protein L38 OS=Homo sapiens	19	1	8.2

Figure 4. THUMPD3 interacts with TRMT112 *in vivo* and *in vitro*. (**A**) Schematic diagram illustrating the principle of immunoprecipitation performed for THUMPD3 by overexpression of THUMPD3 with an HA-tag (THUMPD3-HA) in the *THUMPD3*-KO#1 HEK293T cell line. (**B**) List of the top seven THUMPD3-HA putative interacting proteins identified by mass spectrometry (IP-MS). (**C**) Electrophoresis analysis of immunoprecipitation products of THUMPD3-HA on 12% SDS-PAGE using silver staining; the bands of THUMPD3 and TRMT112 were identified by MS and are indicated. (**D**)The representative tandem mass spectrometry of the peptide MKLLTHNLLSSHVR of TRMT112 proteins obtained by THUMPD3 IP-MS. (**E**) The peptides (colored in red and blue) of TRMT112 identified by THUMPD3 IP-MS. (F and G) Immunoprecipitation (IP) assays showing that THUMPD3-HA can pull down endogenous TRMT112 (**F**) and TRMT112-Flag can pull down endogenous THUMPD3 (**G**). (**H**) The diagrammatic model of *THUMPD3* and *TRMT112* genes co-constructed into pKL-vector and expressed in High Five insect cells. (**I**) The gel filtration chromatography of the THUMPD3–TRMT112 complex on Superdex 200 Increase 10/300 GL column; the peak of the stable complex is indicated by a black asterisk, and the standard molecular weights are marked on the top. (**J**) Electrophoresis analysis of the THUMPD3- TRMT112 complex peak obtained from gel filtration by SDS-PAGE.

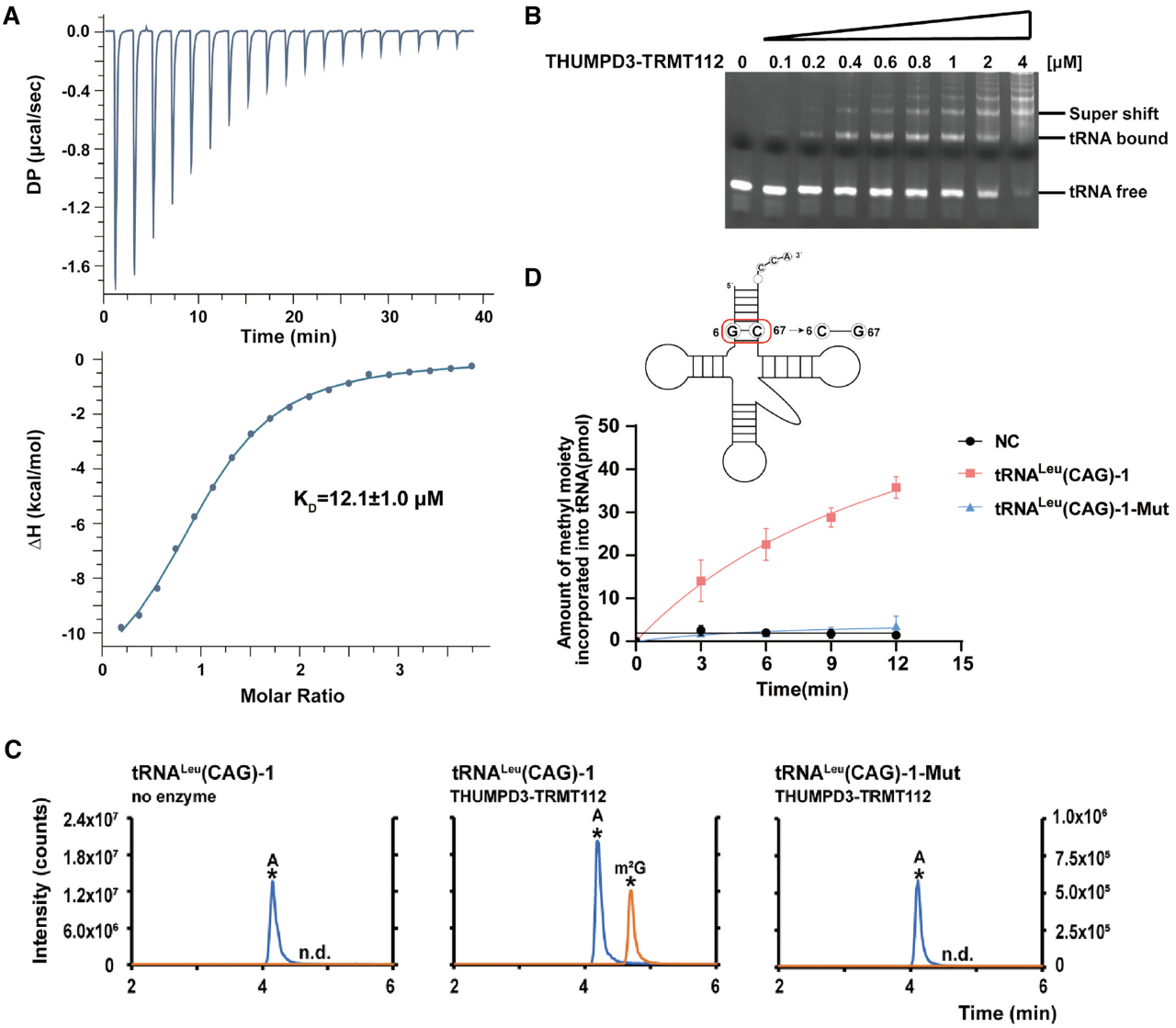

Figure 5. THUMPD3–TRMT112 binary complex catalyzes tRNA:m^{2}G6 modification robustly *in vitro*. (**A**) The sinefungin-binding affinity of the purified THUMPD3–TRMT112 complex as measured by ITC. The K_D value is show in the image. (**B**) The binding affinity of the purified THUMPD3–TRMT112 complex for tRNA^{Leu}(CAG)-1 analyzed by EMSAs. For the reaction, different concentrations of the THUMPD3–TRMT112 complex and 200 nM tRNA^{Leu}(CAG)-1 transcripts were incubated. (**C**) Mass chromatograms of A and m^{2}G from tRNA^{Leu}(CAG)-1 and tRNA^{Leu}(CAG)-1-Mut after incubation with the THUMPD3–TRMT112 complex in the presence of SAM. Target peaks are indicated by black asterisks. n.d., not detectable. The value of left vertical axis stands for the intensity of A and the value of right vertical axis stands for the intensity of m^{2}G. (**D**) The methylation capacity of the purified THUMPD3–TRMT112 complex to tRNA^{Leu}(CAG)-1 and tRNA^{Leu}(CAG)-1-Mut, NC is a negative control to which no RNA was added. The secondary structure of tRNA^{Leu}(CAG)-1 and tRNA^{Leu}(CAG)-1-Mut in which the G6-C67 base pair was mutated into C6-G67, which is shown on the top.

carries a m^{2}G at site 7 (Supplementary Figure S3A) (1,59). To test whether this modification is also catalyzed by THUMPD3. We transcribed hctRNA^{Trp}(CCA)-2 that only differs from bovines' by two-nucleotides and found that it could be methylated by THUMPD3–TRMT112 with m^{2}G *in vitro* (Supplementary Figure S3B). Considering position 6 is C instead of G in both human and bovine tRNA^{Trp}(CCA), the result suggests that THUMPD3–TRMT112 is responsible for m^{2}G7 in this tRNA and probably conserved from bovine to human.

These tested human cytoplasmic tRNAs belong to different tRNA species according to classification by their cognate amino acids, comprising tRNA^{Gly}s, tRNA^{Leu}s, tRNA^{Tyr}s, tRNA^{Asp}s, tRNA^{Glu}s, tRNA^{His}s, tRNA^{Ile}s, tRNA^{Lys}s, tRNA^{Pro}s, tRNA^{Phe}s, tRNA^{Met}s, tRNA^{Arg}s, tRNA^{Thr}s, tRNA^{Ser}s and tRNA^{Trp}. These tRNAs are distinct in their primary sequences, and contain both subtypes of tRNAs, with either a short or long variable loop, while all of them could be catalyzed by the THUMPD3–TRMT112 complex. This indicated that THUMPD3–TRMT112 has a broad specificity for tRNA substrates and does not recognize the specific sequences of different tRNAs. However, the THUMPD3–TRMT112 complex requires the presence of a G at position 6 or 7.

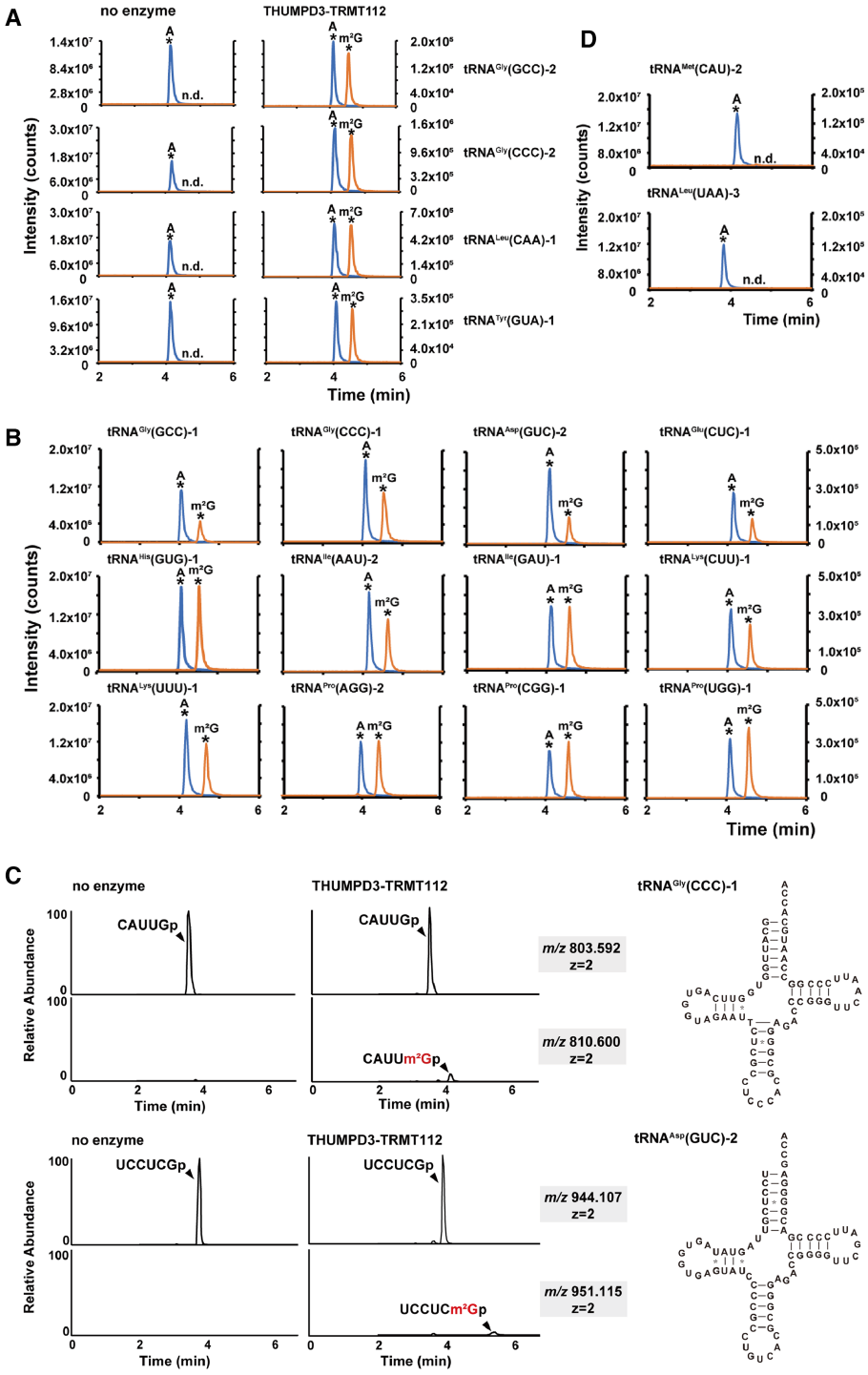

Figure 6. THUMPD3–TRMT112 has a broad range of tRNA substrates. (A and B) Detection of the methylation capability of THUMPD3–TRMT112 to all sixteen human cytoplasmic tRNAs with a G at the sixth position except tRNA^{Leu}(CAG)-1 that had been assayed above. (**A**) Mass chromatograms analysis of A and m^{2}G of tRNA^{Gly}(GCC)-2, tRNA^{Gly}(CCC)-2, tRNA^{Leu}(CAA)-1 and tRNA^{Tyr}(GUA)-1 after incubation with buffer (left panel) or the THUMPD3–TRMT112 complex (right panel) in the presence of SAM. Target peaks are indicated by black asterisks. n.d., not detectable. (**B**) Mass chromatograms of A and m^{2}G of tRNA^{Gly}(GCC)-1, tRNA^{Gly}(CCC)-1, tRNA^{Asp}(GUC)-2, tRNA^{Glu}(CUC)-1, tRNA^{His}(GUG)-1, tRNA^{Ile}(AAU)-2, tRNA^{Ile}(GAU)-1, tRNA^{Lys}(CUU)-1, tRNA^{Lys}(UUU)-1, tRNA^{Pro}(AGG)-2, tRNA^{Pro}(CGG)-1 and tRNA^{Pro}(UGG)-1 after incubation with the THUMPD3–TRMT112 complex in the presence of SAM. (**C**) Extracted-ion chromatograms (XIC) of G6-containing fragments of tRNA^{Gly}(CCC)-1 and tRNA^{Asp}(GUC)-2 digested by RNase T1 without (top) or with (bottom) m^{2}G. The sequences of unmodified and modified fragments are indicated. Target peaks are indicated by black triangle. The *m/z* value and charge state of each fragments and the secondary structure of tRNA^{Gly}(CCC)-1 and tRNA^{Asp}(GUC)-2 are shown on the right. (**D**) Detection of the methylation capability of THUMPD3–TRMT112 to human cytoplasmic tRNAs at which their 6th position is not G. Mass chromatograms analysis of A and m^{2}G of tRNA^{Met}(CAU)-2 and tRNA^{Leu}(UAA)-3 after incubation with the THUMPD3–TRMT112 complex in the presence of SAM. Target peaks are indicated by black asterisks. n.d., not detectable. In A, B and D, the value of left vertical axis stands for the intensity of A and the value of right vertical axis stands for the intensity of m^{2}G.

Characteristic 3′-CCA end and tertiary structure of mature tRNA is crucial for recognition by THUMPD3–TRMT112

We further investigated whether the THUMPD3–TRMT112 complex recognizes some characteristic elements of tRNAs. All mature tRNAs contain a common CCA-tail at their 3′ terminus. Previous studies on Thil (60) and Trm11 (42) showed that the THUMP domain recognizes 3′-CCA end of tRNAs. To determine whether the THUMPD3–TRMT112 complex recognizes the 3′-CCA end to exert its tRNA:m^2G6 formation, we generated a mutant tRNA by deleting its 3′-CCA end and assayed the binding affinity of the THUMPD3–TRMT112 complex to this mutant tRNA using EMSAs (Figure 7A). The results showed that tRNA without a 3′-CCA end could not bind to the THUMPD3–TRMT112 complex, even in the presence of a high concentration of the proteins. Furthermore, no methyltransferase activity of the THUMPD3–TRMT112 complex could be detected when using this tRNA mutant as a substrate (Figure 7B). The results were further supported by RNA-MS analysis (Figure 7C). These results suggested that truncation of the 3′-CCA end of tRNA is deleterious for the recognition and methylation by THUMPD3–TRMT112.

The above results showed that the THUMPD3–TRMT112 complex recognizes G6 and the 3′-CCA end of their substrate tRNAs. Notably, 5′-tRF harbors G6 but lacks the 3′-CCA end compared with full length tRNA. To verify whether the THUMPD3–TRMT112 complex could catalyze m^2G formation in the tRNA fragment after cleavage, we generated a 5′-tRF of $tRNA^{Gly}$(GCC), which is one of the most abundant sperm tRFs (37). As expected, no m^2G could be formed on 5′-tRF in contrast to the mature $tRNA^{Gly}$(GCC) (Figure 7D (left and middle panel)). Further, to investigate whether the tertiary structure of tRNA is required for recognition, we generated a tRNA-mini-helix harboring the G6 and 3′-CCA end by retaining the acceptor stem and anticodon stem loop. The methylation activity of the THUMPD3–TRMT112 complex toward this mini-helix was assayed (Figure 7D (right panel)). RNA-MS analysis showed that the THUMPD3–TRMT112 complex exerted no methyltransferase activity toward the mini-helix of $tRNA^{Gly}$(GCC), suggesting that the tRNA tertiary structure is essential for recognition by the modifying enzyme.

To better understand the recognition mechanism of THUMPD3–TRMT112, we generated a tertiary structure model of the human THUMPD3–TRMT112 complex. The structural model of THUMPD3 was built based on the structures of the *Tt*TrmN and *Pf*Trm14 (PDB codes: 3TMA and 3TM4) using the automated protein structure homology-modelling server, I-TASSER (44,61–63). The model of the THUMPD3–TRMT112 complex was generated by manually docking TRMT112 from the crystal structure of the human METTL5–TRMT112 complex (PDB code: 6H2V) onto the THUMPD3 model through structural superimposition (64) (Figure 7E). In this model, TRMT112 binds to the opposite surface of the SAM-binding pocket of the MTase domain of THUMPD3, and has no direct contact with the THUMP domain. The binding mode of TRMT112 to the MTase domain of THUMPD3 is similar to that observed in other known MTase-Trm112 complexes, such as Bud23-Trm112 (65) and Trm9-Trm112 (66). Complex formation involves a large surface area formed by THUMPD3 and TRMT112, and the interface is characterized by the presence of a large hydrophobic patch on THUMPD3, which might explain why standalone THUMPD3 tends to polymerize *in vitro*. In this model, the THUMP domain locates near to the SAM-binding pocket of THUMPD3, suggesting that this THUMP domain might also be involved in recognizing the 3′-CCA end of tRNA substrates, as in Thil (60)and Trm11 (42). Thus, the available structural model suggested that the THUMP domain, but not TRMT112, is more likely to be involved in the recognition of the 3′-CCA end.

THUMPD3 is widely expressed in various tissues and is important for protein translation and cell proliferation

THUMPD3 had barely been characterized before; therefore, we determined the expression of THUMPD3 in different human cell lines and mouse tissues (Figure 8A and B). In the nine human cell lines tested (HEK293T, Hep G2, HGC-27, HeLa, MCF-7, MDA-MB-231, MDA-MB-453, SKOV2 and A549), which were from human embryonic kidney, liver, stomach, cervix uterus, breast, ovary, and lung, respectively, *THUMPD3* was expressed in all the tested cell lines (Figure 8A). From the tissues of 8-week old mice (brain, heart, kidney, liver, lung, muscle, spleen and testis), we found that *Thumpd3* mRNA is highly expressed in all these tissues, with extremely high expression in the testis (Figure 8B and Supplementary Figure S4). *Thumpd3* expression in the testis was >20-fold higher than that in other tissues, including the brain, heart, kidney, liver, lung, muscle, and spleen. Meanwhile, we also detected the expression of *Trmt112* in mouse tissues, and the result showed that *Trmt112* is also highly expressed in all the eight tested tissues, especially in the testis (Supplementary Figure S5). Further, we performed protein sequence alignment of THUMPD3 proteins from eukaryotes (67), and found that THUMPD3 is present in metazoans and has a highly conserved primary sequence, suggesting a conserved role during evolution (Supplementary Figure S6).

We next asked whether THUMPD3 has any physiological importance in human cells. To investigate whether THUMPD3 affects protein synthesis, we performed polysome profiling on a sucrose gradient. The results showed that the level of polysomes was reduced in both the *THUMPD3* KO cell lines (*THUMPD3*-KO#1 and *THUMPD3*-KO#2) compared with that in WT cells, suggesting strong suppression of global translation (Figure 8C). To verify the role of THUMPD3 in cell proliferation, we performed cell counting kit-8 assays to determine the cell growth rate of *THUMPD3* KO and WT cells (Figure 8D). Compared with that in WT cells, a noticeable decrease in cell proliferation was observed in both of the *THUMPD3* KO cell lines, indicating that THUMPD3 plays a role in cell proliferation.

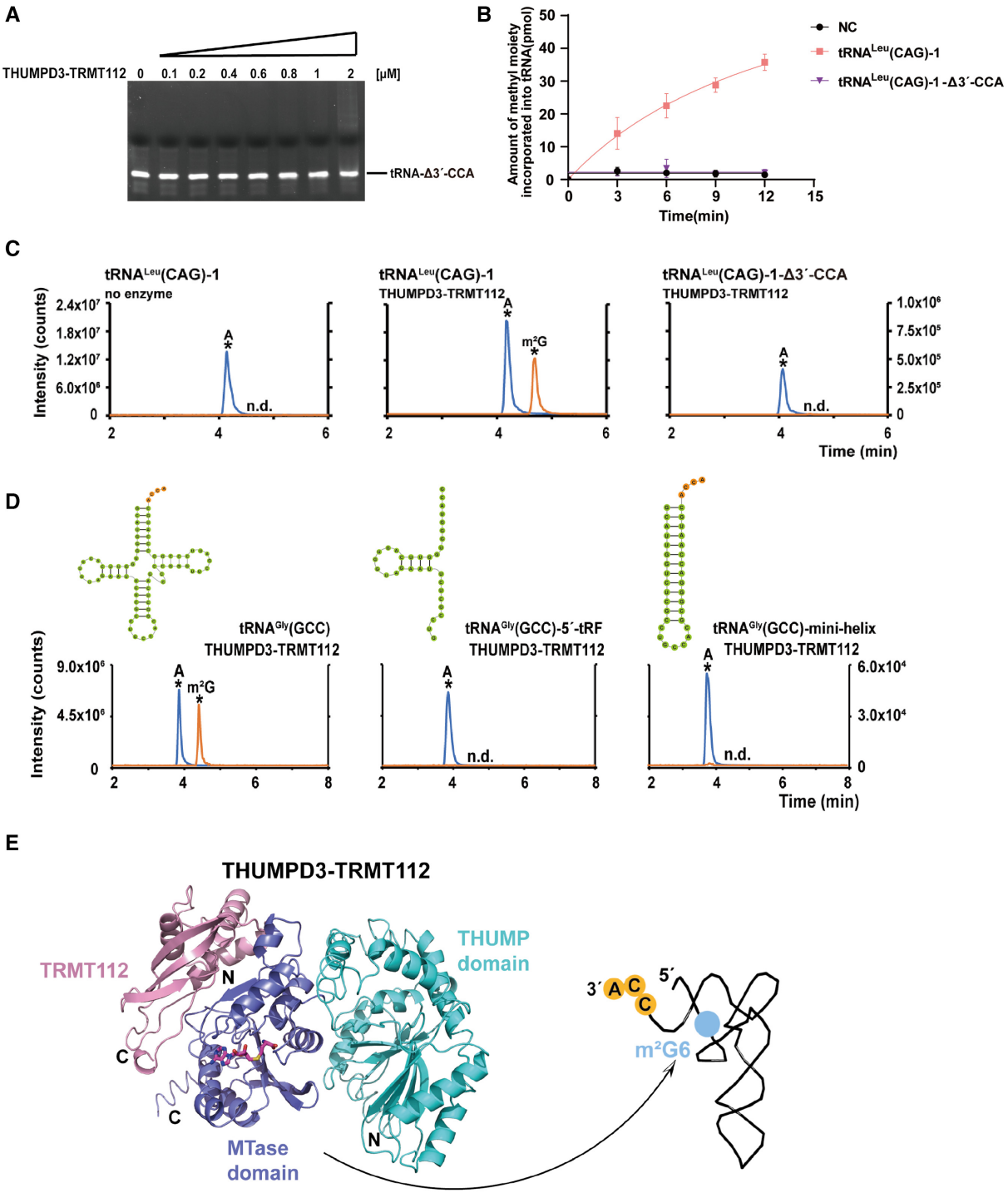

Figure 7. Characteristic 3′-CCA end and tertiary structure of mature tRNA are crucial for recognition by THUMPD3–TRMT112. (**A**) The binding affinity of the purified THUMPD3–TRMT112 complex for $tRNA^{Leu}$(CAG)-1-Δ3′-CCA analyzed by EMSAs. For the reaction, different concentrations of the THUMPD3–TRMT112 complex and 200 nM $tRNA^{Leu}$(CAG)-1-Δ3′-CCA transcripts were incubated. (**B**) The methyltransferase activity assays of the purified THUMPD3–TRMT112 complex to $tRNA^{Leu}$(CAG)-1 and $tRNA^{Leu}$(CAG)-1-Δ3′-CCA. (**C**) Mass chromatograms of A and m^2G of $tRNA^{Leu}$(CAG)-1 and $tRNA^{Leu}$(CAG)-1-Δ3′-CCA after incubation with the THUMPD3–TRMT112 complex in the presence of SAM. Target peaks are indicated by black asterisks. n.d., not detectable. (**D**) Mass chromatograms of A and m^2G of $tRNA^{Gly}$(GCC), $tRNA^{Gly}$(GCC)-5′-tRF and $tRNA^{Gly}$(GCC)-mini-helix after incubation with THUMPD3–TRMT112 in the presence of SAM. Target peaks are indicated by black asterisks. n.d., not detectable. In C and D, the value of left vertical axis stands for the intensity of A and the value of right vertical axis stands for the intensity of m^2G. The secondary structure of mature $tRNA^{Gly}$(GCC) which contains accept stem, D loop, anticodon stem loop, variable loop, and TΨC loop; 5′-tRF, which comprises the 5′-half of $tRNA^{Gly}$(GCC) containing 34 nucleotides (nt); and the mini-helix, which contains accept stem and anticodon stem loop of $tRNA^{Gly}$(GCC), are showed on the top left. (**E**) The catalytic model of THUMPD3–TRMT112 with substrate tRNAs. The structural model of the THUMPD3–TRMT112 complex was generated by a protein structure homology-modelling server combined with manual structural superimposition and docking. The model is shown in cartoon form, and the MTase and THUMP domain of THUMPD3 plus TRMT112 are indicated in different colors.

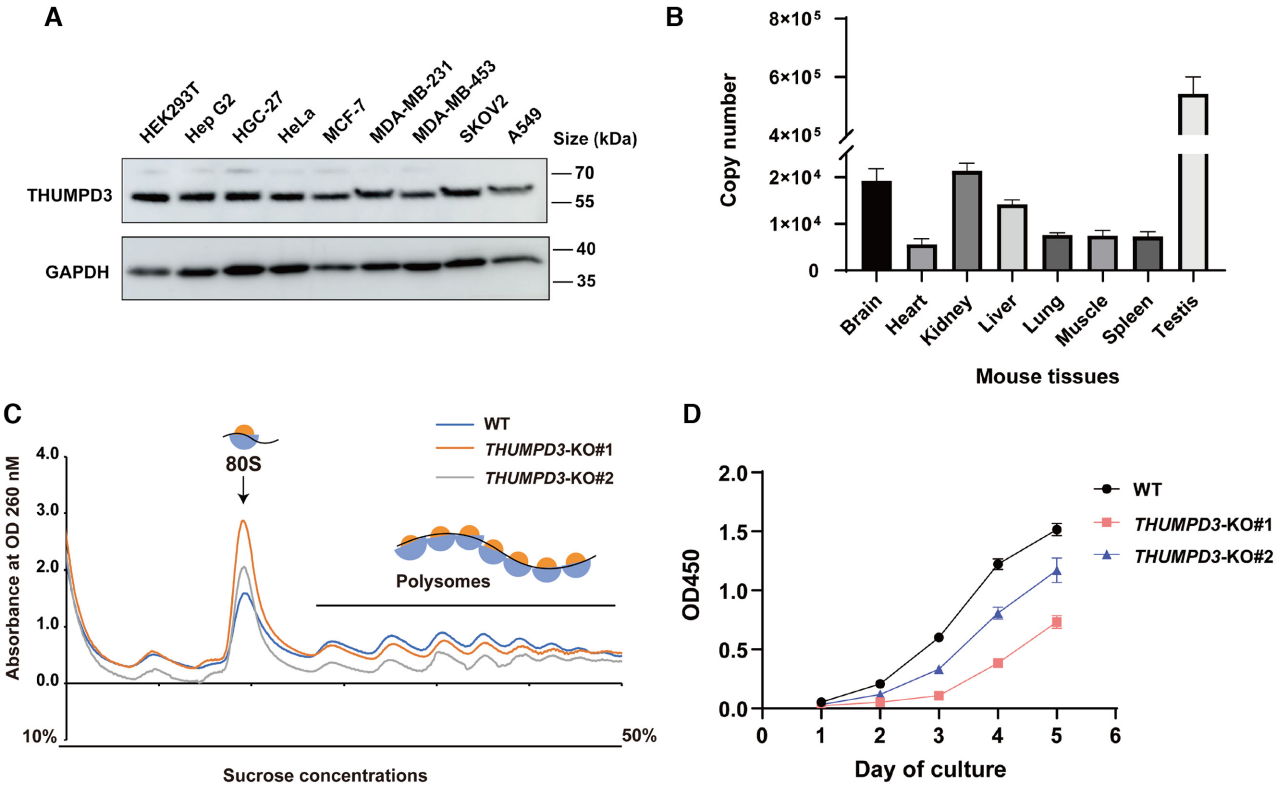

Figure 8. THUMPD3 is widely expressed and is crucial for protein translation and cell proliferation. (**A**) The protein level of THUMPD3 in different human cell lines (HEK293T, Hep G2, HGC-27, HeLa, MCF-7, MDA-MB-231, MDA-MB-453, SKOV2 and A549) analyzed by western blotting. (**B**) The copy number of *Thumpd3* mRNA in different mouse tissues (brain, heart, kidney, liver, lung, muscle, spleen, and testis) measured by absolute quantitative real-time PCR (qRT-PCR). (**C**) The polysome profiling of WT, *THUMPD3*-KO#1 and *THUMPD3*-KO#2 HEK293T cell lines were analyzed. (**D**) The growth rate curve of WT, *THUMPD3*-KO#1 and *THUMPD3*-KO#2 HEK293T cell lines under normal culture conditions assayed using Cell Counting Kit-8 (CCK-8) proliferation analysis.

DISCUSSION

THUMP domain in tRNA recognition and modification

Here, we showed that the two protein subunits, THUMPD3 and an auxiliary protein TRMT112, are responsible for the generation of $m^2G6/7$ in human tRNAs. THUMPD3 acts as the catalytic subunit, which possesses an N-terminal THUMP domain linked to a C-terminal RFM domain. The Rossman-fold MTase belongs to Class I SAM-dependent MTases superfamily, and represents the majority of RNA MTases (24,68). The THUMP domain is an ancient RNA-binding domain that is universal in the three kingdoms of life. It could link to several types of catalytic domains to engage in different tRNA modifications. CDAT8 is involved in 'C-to-U' editing at tRNA position 8 in archaea to maintain tRNA tertiary structures, which possesses an N-terminal cytidine deaminase domain, a central ferredoxin-like domain (FLD), and a C-terminal THUMP domain (69). ThiI catalyzes the tRNA:s^4U8 modification in some prokaryotes to act as a sensor to response UV exposure, which contains an N-terminal FLD (NFLD) with a THUMP domain and C-terminal PP-loop pyrophosphatase domain (60). Trm11 possesses an N-terminal THUMP domain and a C-terminal RFM domain (70). NFLD is regarded as a small subunit belonging to the THUMP domain. However, archaeal PUS10, which produces a pseudouridine modification at the 54^{th} and 55^{th} positions in tRNAs, possesses a Psi synthase catalytic domain and a THUMP domain without an NFLD (71). Here, we showed that THUMPD3–TRMT112 recognizes the characteristic 3′-CCA end of tRNAs. Similarly, the 3′-CCA end was also recognized by ThiI, CDAT8, and Trm11 in tRNA modifications, indicating that binding with the 3′-CCA end is a common feature of THUMP domain. While the tertiary structures of a large number of THUMP domain-containing proteins await to be solved and we could not exclude the possibility of different RNA recognition mechanism of THUMP domain.

From standalone protein to multiprotein complex: the evolution of tRNA modifying enzymes

In contrast to Trm14 or TrmN (33,44), standalone human THUMPD3 is catalytically inactive *in vitro*. TRMT112 is a small protein without an MTase catalytic domain. We showed that TRMT112 is required for THUMPD3 to be catalytically active. TRMT112 not only promotes the SAM-binding capability of THUMPD3, but also functions in the protein stabilization of THUMPD3, probably by masking the hydrophobic regions. Interestingly, the crucial role of Trm112 for Trm11 is also observed in eukaryotes (34), and the activation mechanism of Trm112 was comprehensively deciphered by Graille's group (42). They showed that

Trm112 influences both the SAM-binding and the tRNA-binding of Trm11. During evolution, many other tRNA modifying enzymes also form multiprotein complexes in eukaryotes. By contrast, in lower species, a single modifying enzyme usually catalyze the same tRNA modification on their own, e.g. Trm7/Trm732 or Trm7/Trm734 in eukaryotes versus TrmJ or TrmL in bacteria for the Nm32 or Nm34 of tRNAs (72); and Trm6/Trm61 in eukaryotes versus TrmI in bacteria for the m^1A58 of tRNAs (73,74). The role of the auxiliary proteins varies in the formation of tRNA modifications; however, the physiological function and the nature of evolution from a simple enzyme to complicated modifying complexes remain largely unexplored.

Besides THUMPD3 and Trm11, several other RNA and protein MTases use Trm112/TRMT112 as an auxiliary subunit (75) (Supplementary Figure S7). Trm9-Trm112 modifies mcm^5U at a wobble position to ensure accurate codon pairing and promote translation fidelity (76,77). Bud23-Trm112 and METTL5-TRMT112 modify m^7G or m^6A on 18S rRNA in eukaryotes (64,78), respectively. Moreover, human HEMK2-TRMT112 methylates histone H4 and eRF1 (79,80). The reason why all these MTases recruit a common Trm112/ TRMT112 activator remains unclear. One could speculate that such an auxiliary protein-centered regulation might facilitate regulatory networks in organisms and be more economical in bio-utilization process in higher eukaryotes.

Biological role of THUMPD3 and tRNA:m^2G6 modification

THUMPD3–TRMT112 has a broad specificity for mature human cytoplasmic tRNAs. Moreover, THUMPD3 is widely expressed in human cell lines and mouse tissues, and is conserved in metazoans, suggesting an important role of THUMPD3. Knocking out of *THUMPD3* hampered cell proliferation and global protein synthesis in HEK293T cells, emphasizing the critical biological functions of THUMPD3. However, the mechanistic role of THUMPD3 and the widespread presence of tRNA:m^2G6 in cell remain to be investigated. The m^2G modification of tRNA predominantly occurs at the 6^{th} and 10^{th} positions in higher eukaryotes; however, no obvious phenotypes were observed after the deletion of *Trm11* in yeast (34), suggesting a different role of THUMPD3 and Trm11.

Recent reports showed that 5′-tRFs were increased in parental sperm in HFD mice compared with those normal mice, together with a markedly elevated level of m^2G and m^5C modifications(29). The biological function of m^5C in tRNA and tRF has been extensively studied in mammals (30,31), while the mechanistic role of m^2G was barely studied. Interestingly, we found that THUMPD3 was expressed at extremely high levels in the testis, hinting a potential association of THUMPD3 and the m^2G modification in sperm tRF. Moreover, m^2G6 is located in the 5′-half of the tRNA molecule, and thus could be confer to 5′-tRFs after cleavage. As we showed above, with the deletion of *THUMPD3*, the level of m^2G became undetectable in $tRNA^{Gly}$(CCC) and $tRNA^{Gly}$(GCC). Those tRNAs were two of the most abundant 5′-tRFs species derived from mature tRNAs after the cleavage by angiogenin *in vivo* (81), suggesting that m^2G6, instead of m^2G10, is the main source of m^2G modification in these two 5′-tRFs. However, the biogenesis of sperm tRFs is unclear. The exact role of THUMPD3 in the formation of m^2G in sperm 5′-tRFs and intergenerational inheritance is not yet known, although the results of the present study suggest that it worth further exploration.

SUPPLEMENTARY DATA

Supplementary Data are available at NAR Online.

ACKNOWLEDGEMENTS

We thank the Molecular and Cell Biology Core Facility (MCBCF), the Multi-Omics Core Facility (MOCF), and the Molecular Imaging Core Facility (MICF) at the School of Life Science and Technology, ShanghaiTech University for providing technical support. We also thank the Analytical Chemistry platform (ShanghaiTech University, SIAIS) for technical assistance with protein identification by MS. We thank Prof. Bei Yang and Prof. Jun Liao at ShanghaiTech University for providing High Five and Sf9 insect cells.

Author contributions: R.-J.L. and W.-Q.Y. conceived the ideas for this work. Q.-P.X. performed *in vitro* assays for methyltransferase activity using ^3H-isotope. J.-Y.G. performed absolute quantitative real-time PCR assays with W.-Q.Y. Y.N. provided technological support for Baculovirus Expression System. X.L., D.L. and H.L. (Huan Lin) performed LC–ESI-MS for RNA fragment analysis. W.-Q.Y. performed all other experiments with technical help from H.L. (Hao Li), W.-Y.Z. and J.L. R.-J.L. and W.-Q.Y. wrote the manuscript, which was reviewed by all authors.

FUNDING

National Key Research and Development Program of China [2020YFA0803400]; National Natural Science Foundation of China [32022040, 31971230, 31770842]. Funding for open access charge: National Natural Science Foundation of China [32022040, 31971230, 31770842].

Conflict of interest statement. None declared.

REFERENCES

1. Boccaletto,P., Machnicka,M.A., Purta,E., Piatkowski,P., Baginski,B., Wirecki,T.K., de Crécy-Lagard,V., Ross,R., Limbach,P.A., Kotter,A. *et al.* (2018) MODOMICS: a database of RNA modification pathways. 2017 update. *Nucleic Acids Res.*, **46**, D303–D307.
2. El Yacoubi,B., Bailly,M. and de Crécy-Lagard,V. (2012) Biosynthesis and function of posttranscriptional modifications of transfer RNAs. *Annu Rev. Genet.*, **46**, 69–95.
3. Pan,T. (2018) Modifications and functional genomics of human transfer RNA. *Cell Res.*, **28**, 395–404.
4. Phizicky,E.M. and Hopper,A.K. (2010) tRNA biology charges to the front. *Genes Dev.*, **24**, 1832–1860.
5. de Crécy-Lagard,V., Boccaletto,P., Mangleburg,C.G., Sharma,P., Lowe,T.M., Leidel,S.A. and Bujnicki,J.M. (2019) Matching tRNA modifications in humans to their known and predicted enzymes. *Nucleic Acids Res.*, **47**, 2143–2159.
6. Motorin,Y. and Helm,M. (2010) tRNA stabilization by modified nucleotides. *Biochemistry*, **49**, 4934–4944.
7. Klassen,R., Bruch,A. and Schaffrath,R. (2017) Independent suppression of ribosomal +1 frameshifts by different tRNA anticodon loop modifications. *RNA Biol.*, **14**, 1252–1259.

8. Rozov,A., Demeshkina,N., Khusainov,I., Westhof,E., Yusupov,M. and Yusupova,G. (2016) Novel base-pairing interactions at the tRNA wobble position crucial for accurate reading of the genetic code. *Nat. Commun.*, **7**, 10457.
9. Guzzi,N., Cieśla,M., Ngoc,P.C.T., Lang,S., Arora,S., Dimitriou,M., Pimková,K., Sommarin,M.N.E., Munita,R., Lubas,M. *et al.* (2018) Pseudouridylation of tRNA-derived fragments steers translational control in stem cells. *Cell*, **173**, 1204–1216.
10. Freund,I., Buhl,D.K., Boutin,S., Kotter,A., Pichot,F., Marchand,V., Vierbuchen,T., Heine,H., Motorin,Y., Helm,M. *et al.* (2019) 2′-*O*-methylation within prokaryotic and eukaryotic tRNA inhibits innate immune activation by endosomal Toll-like receptors but does not affect recognition of whole organisms. *RNA*, **25**, 869–880.
11. Laxman,S., Sutter,B.M., Wu,X., Kumar,S., Guo,X., Trudgian,D.C., Mirzaei,H. and Tu,B.P. (2013) Sulfur amino acids regulate translational capacity and metabolic homeostasis through modulation of tRNA thiolation. *Cell*, **154**, 416–429.
12. Zhang,Y., Zhang,X., Shi,J., Tuorto,F., Li,X., Liu,Y., Liebers,R., Zhang,L., Qu,Y., Qian,J. *et al.* (2018) Dnmt2 mediates intergenerational transmission of paternally acquired metabolic disorders through sperm small non-coding RNAs. *Nat. Cell Biol.*, **20**, 535–540.
13. Chujo,T. and Tomizawa,K. (2021) Human transfer RNA modopathies: diseases caused by aberrations in transfer RNA modifications. *FEBS J.*, https://doi.org/10.1111/febs.15736.
14. Jonkhout,N., Tran,J., Smith,M.A., Schonrock,N., Mattick,J.S. and Novoa,E.M. (2017) The RNA modification landscape in human disease. *RNA*, **23**, 1754–1769.
15. Torres,A.G., Batlle,E. and Ribas de Pouplana,L. (2014) Role of tRNA modifications in human diseases. *Trends Mol Med.*, **20**, 306–314.
16. Hurwitz,J., Gold,M. and Anders,M. (1964) The enzymatic methylation of ribonucleic acid and deoxyribonucleic acid. 3. purification of soluble ribonucleic acid methylating enzymes. *J. Biol. Chem.*, **239**, 3462–3473.
17. Goto-Ito,S., Ito,T., Kuratani,M., Bessho,Y. and Yokoyama,S. (2009) Tertiary structure checkpoint at anticodon loop modification in tRNA functional maturation. *Nat. Struct. Mol. Biol.*, **16**, 1109–1115.
18. Rubio,M.A., Gaston,K.W., McKenney,K.M., Fleming,I.M., Paris,Z., Limbach,P.A. and Alfonzo,J.D. (2017) Editing and methylation at a single site by functionally interdependent activities. *Nature*, **542**, 494–497.
19. Liu,R.J., Zhou,M., Fang,Z.P., Wang,M., Zhou,X.L. and Wang,E.D. (2013) The tRNA recognition mechanism of the minimalist SPOUT methyltransferase, TrmL. *Nucleic Acids Res.*, **41**, 7828–7842.
20. Guy,M.P., Podyma,B.M., Preston,M.A., Shaheen,H.H., Krivos,K.L., Limbach,P.A., Hopper,A.K. and Phizicky,E.M. (2012) Yeast Trm7 interacts with distinct proteins for critical modifications of the $tRNA^{Phe}$ anticodon loop. *RNA*, **18**, 1921–1933.
21. Zhou,M., Long,T., Fang,Z.P., Zhou,X.L., Liu,R.J. and Wang,E.D. (2015) Identification of determinants for tRNA substrate recognition by *Escherichia coli* C/U34 2′-*O*-methyltransferase. *RNA Biol.*, **12**, 900–911.
22. Wiener,D. and Schwartz,S. (2021) The epitranscriptome beyond m^6A. *Nat. Rev. Genet.*, **22**, 119–131.
23. Li,X., Xiong,X. and Yi,C. (2016) Epitranscriptome sequencing technologies: decoding RNA modifications. *Nat. Methods.*, **14**, 23–31.
24. Hori,H. (2014) Methylated nucleosides in tRNA and tRNA methyltransferases. *Front. Genet.*, **5**, 144.
25. Barraud,P. and Tisné,C. (2019) To be or not to be modified: Miscellaneous aspects influencing nucleotide modifications in tRNAs. *IUBMB Life*, **71**, 1126–1140.
26. Pallan,P.S., Kreutz,C., Bosio,S., Micura,R. and Egli,M. (2008) Effects of N^2,N^2-dimethylguanosine on RNA structure and stability: crystal structure of an RNA duplex with tandem $m^2{}_2G$:A pairs. *RNA*, **14**, 2125–2135.
27. Dai,Q., Zheng,G., Schwartz,M.H., Clark,W.C. and Pan,T. (2017) Selective enzymatic demethylation of N^2,N^2-Dimethylguanosine in RNA and its application in high-throughput tRNA sequencing. *Angew. Chem. Int. Ed. Engl.*, **56**, 5017–5020.
28. Chan,C.T., Dyavaiah,M., DeMott,M.S., Taghizadeh,K., Dedon,P.C. and Begley,T.J. (2010) A quantitative systems approach reveals dynamic control of tRNA modifications during cellular stress. *PLoS Genet.*, **6**, e1001247.
29. Chen,Q., Yan,M., Cao,Z., Li,X., Zhang,Y., Shi,J., Feng,G.H., Peng,H., Zhang,X., Zhang,Y. *et al.* (2016) Sperm tsRNAs contribute to intergenerational inheritance of an acquired metabolic disorder. *Science*, **351**, 397–400.
30. Tuorto,F., Liebers,R., Musch,T., Schaefer,M., Hofmann,S., Kellner,S., Frye,M., Helm,M., Stoecklin,G. and Lyko,F. (2012) RNA cytosine methylation by Dnmt2 and NSun2 promotes tRNA stability and protein synthesis. *Nat. Struct. Mol. Biol.*, **19**, 900–905.
31. Kiani,J., Grandjean,V., Liebers,R., Tuorto,F., Ghanbarian,H., Lyko,F., Cuzin,F. and Rassoulzadegan,M. (2013) RNA-mediated epigenetic heredity requires the cytosine methyltransferase Dnmt2. *PLoS Genet.*, **9**, e1003498.
32. Jühling,F., Mörl,M., Hartmann,R.K., Sprinzl,M., Stadler,P.F. and Pütz,J. (2009) tRNAdb 2009: compilation of tRNA sequences and tRNA genes. *Nucleic Acids Res.*, **37**, D159–D162.
33. Menezes,S., Gaston,K.W., Krivos,K.L., Apolinario,E.E., Reich,N.O., Sowers,K.R., Limbach,P.A. and Perona,J.J. (2011) Formation of m^2G6 in *Methanocaldococcus jannaschii* tRNA catalyzed by the novel methyltransferase Trm14. *Nucleic Acids Res.*, **39**, 7641–7655.
34. Purushothaman,S.K., Bujnicki,J.M., Grosjean,H. and Lapeyre,B. (2005) Trm11p and Trm112p are both required for the formation of 2-methylguanosine at position 10 in yeast tRNA. *Mol. Cell Biol.*, **25**, 4359–4370.
35. Edqvist,J., Blomqvist,K. and Stråby,K.B. (1994) Structural elements in yeast tRNAs required for homologous modification of guanosine-26 into dimethylguanosine-26 by the yeast Trm1 tRNA-modifying enzyme. *Biochemistry*, **33**, 9546–9551.
36. Awai,T., Kimura,S., Tomikawa,C., Ochi,A., Ihsanawati, Bessho,Y., Yokoyama,S., Ohno,S., Nishikawa,K., Yokogawa,T. *et al.* (2009) *Aquifex aeolicus* tRNA (N^2,N^2-guanine)-dimethyltransferase (Trm1) catalyzes transfer of methyl groups not only to guanine 26 but also to guanine 27 in tRNA. *J. Biol. Chem.*, **284**, 20467–20478.
37. Tosar,J.P., Gámbaro,F., Darré,L., Pantano,S., Westhof,E. and Cayota,A. (2018) Dimerization confers increased stability to nucleases in 5′ halves from glycine and glutamic acid tRNAs. *Nucleic Acids Res.*, **46**, 9081–9093.
38. Edqvist,J., Stråby,K.B. and Grosjean,H. (1995) Enzymatic formation of N^2,N^2-dimethylguanosine in eukaryotic tRNA: importance of the tRNA architecture. *Biochimie*, **77**, 54–61.
39. Arimbasseri,A.G., Blewett,N.H., Iben,J.R., Lamichhane,T.N., Cherkasova,V., Hafner,M. and Maraia,R.J. (2015) RNA polymerase III output is functionally linked to tRNA dimethyl-G26 modification. *PLoS Genet.*, **11**, e1005671.
40. Blaesius,K., Abbasi,A.A., Tahir,T.H., Tietze,A., Picker-Minh,S., Ali,G., Farooq,S., Hu,H., Latif,Z., Khan,M.N. *et al.* (2018) Mutations in the tRNA methyltransferase 1 gene TRMT1 cause congenital microcephaly, isolated inferior vermian hypoplasia and cystic leukomalacia in addition to intellectual disability. *Am. J. Med. Genet. A*, **176**, 2517–2521.
41. Hirata,A., Suzuki,T., Nagano,T., Fujii,D., Okamoto,M., Sora,M., Lowe,T.M., Kanai,T., Atomi,H., Suzuki,T. *et al.* (2019) Distinct modified nucleosides in $tRNA^{Trp}$ from the hyperthermophilic archaeon *Thermococcus kodakarensis* and requirement of tRNA $m^2G10/m^2{}_2G10$ methyltransferase (Archaeal Trm11) for survival at high temperatures. *J. Bacteriol.*, **201**, e00448-19.
42. Bourgeois,G., Marcoux,J., Saliou,J.M., Cianférani,S. and Graille,M. (2017) Activation mode of the eukaryotic m^2G10 tRNA methyltransferase Trm11 by its partner protein Trm112. *Nucleic Acids Res.*, **45**, 1971–1982.
43. Wolff,P., Villette,C., Zumsteg,J., Heintz,D., Antoine,L., Chane-Woon-Ming,B., Droogmans,L., Grosjean,H. and Westhof,E. (2020) Comparative patterns of modified nucleotides in individual tRNA species from a mesophilic and two thermophilic archaea. *RNA*, **26**, 1957–1975.
44. Fislage,M., Roovers,M., Tuszynska,I., Bujnicki,J.M., Droogmans,L. and Versées,W. (2012) Crystal structures of the tRNA:m^2G6 methyltransferase Trm14/TrmN from two domains of life. *Nucleic Acids Res.*, **40**, 5149–5161.
45. Aravind,L. and Koonin,E.V. (2001) THUMP–a predicted RNA-binding domain shared by 4-thiouridine, pseudouridine synthases and RNA methylases. *Trends Biochem. Sci.*, **26**, 215–217.
46. Armengaud,J., Urbonavicius,J., Fernandez,B., Chaussinand,G., Bujnicki,J.M. and Grosjean,H. (2004) N^2-methylation of guanosine at position 10 in tRNA is catalyzed by a THUMP domain-containing,

S-adenosylmethionine-dependent methyltransferase, conserved in Archaea and Eukaryota. *J. Biol. Chem.*, **279**, 37142–37152.
47. Fitzgerald,D.J., Berger,P., Schaffitzel,C., Yamada,K., Richmond,T.J. and Berger,I. (2006) Protein complex expression by using multigene baculoviral vectors. *Nat. Methods.*, **3**, 1021–1032.
48. Trowitzsch,S., Bieniossek,C., Nie,Y., Garzoni,F. and Berger,I. (2010) New baculovirus expression tools for recombinant protein complex production. *J. Struct. Biol.*, **172**, 45–54.
49. Wu,Y., Liang,D., Wang,Y., Bai,M., Tang,W., Bao,S., Yan,Z., Li,D. and Li,J. (2013) Correction of a genetic disease in mouse via use of CRISPR-Cas9. *Cell Stem Cell*, **13**, 659–662.
50. Huang,Q., Yao,P., Eriani,G. and Wang,E.D. (2012) *In vivo* identification of essential nucleotides in $tRNA^{Leu}$ to its functions by using a constructed yeast $tRNA^{Leu}$ knockout strain. *Nucleic Acids Res.*, **40**, 10463–10477.
51. Chan,P.P. and Lowe,T.M. (2016) GtRNAdb 2.0: an expanded database of transfer RNA genes identified in complete and draft genomes. *Nucleic Acids Res.*, **44**, D184–D189.
52. Li,Y., Chen,J., Wang,E. and Wang,Y. (1999) T7 RNA polymerase transcription of *Escherichia coli* isoacceptors $tRNA^{Leu}$. *Sci. China C Life Sci.*, **42**, 185–190.
53. Kibbe,W.A. (2007) OligoCalc: an online oligonucleotide properties calculator. *Nucleic Acids Res.*, **35**, W43–W46.
54. Gandin,V., Sikström,K., Alain,T., Morita,M., McLaughlan,S., Larsson,O. and Topisirovic,I. (2014) Polysome fractionation and analysis of mammalian translatomes on a genome-wide scale. *J. Vis. Exp.*, **87**, 51455.
55. Li,J., Wang,Y.N., Xu,B.S., Liu,Y.P., Zhou,M., Long,T., Li,H., Dong,H., Nie,Y., Chen,P.R. *et al.* (2020) Intellectual disability-associated gene *ftsj1* is responsible for 2′-*O*-methylation of specific tRNAs. *EMBO Rep.*, **21**, e50095.
56. Kadaba,S., Krueger,A., Trice,T., Krecic,A.M., Hinnebusch,A.G. and Anderson,J. (2004) Nuclear surveillance and degradation of hypomodified initiator $tRNA^{Met}$ in *S. cerevisiae*. *Genes Dev.*, **18**, 1227–1240.
57. Guy,M.P. and Phizicky,E.M. (2014) Two-subunit enzymes involved in eukaryotic post-transcriptional tRNA modification. *RNA Biol.*, **11**, 1608–1618.
58. Suzuki,T., Ikeuchi,Y., Noma,A., Suzuki,T. and Sakaguchi,Y. (2007) Mass spectrometric identification and characterization of RNA-modifying enzymes. *Methods Enzymol.*, **425**, 211–229.
59. Keith,G. and Heyman,T. (1990) Heterogeneities in vertebrate $tRNAs^{Trp}$ avian retroviruses package only as a primer the $tRNA^{Trp}$ lacking modified m^2G in position 7. *Nucleic Acids Res.*, **18**, 703–710.
60. Waterman,D.G., Ortiz-Lombardía,M., Fogg,M.J., Koonin,E.V. and Antson,A.A. (2006) Crystal structure of *Bacillus anthracis* ThiI, a tRNA-modifying enzyme containing the predicted RNA-binding THUMP domain. *J. Mol. Biol.*, **356**, 97–110.
61. Roy,A., Kucukural,A. and Zhang,Y. (2010) I-TASSER: a unified platform for automated protein structure and function prediction. *Nat Protoc.*, **5**, 725–738.
62. Yang,J., Yan,R., Roy,A., Xu,D., Poisson,J. and Zhang,Y. (2015) The I-TASSER Suite: protein structure and function prediction. *Nat. Methods.*, **12**, 7–8.
63. Yang,J. and Zhang,Y. (2015) I-TASSER server: new development for protein structure and function predictions. *Nucleic Acids Res.*, **43**, W174–W181.
64. van Tran,N., Ernst,F.G.M., Hawley,B.R., Zorbas,C., Ulryck,N., Hackert,P., Bohnsack,K.E., Bohnsack,M.T., Jaffrey,S.R., Graille,M. *et al.* (2019) The human 18S rRNA m^6A methyltransferase METTL5 is stabilized by TRMT112. *Nucleic Acids Res.*, **47**, 7719–7733.
65. Létoquart,J., Huvelle,E., Wacheul,L., Bourgeois,G., Zorbas,C., Graille,M., Heurgué-Hamard,V. and Lafontaine,D.L. (2014) Structural and functional studies of Bud23-Trm112 reveal 18S rRNA N7-G1575 methylation occurs on late 40S precursor ribosomes. *Proc. Natl. Acad. Sci. U.S.A.*, **111**, E5518–E5526.
66. Létoquart,J., van Tran,N., Caroline,V., Aleksandrov,A., Lazar,N., van Tilbeurgh,H., Liger,D. and Graille,M. (2015) Insights into molecular plasticity in protein complexes from Trm9-Trm112 tRNA modifying enzyme crystal structure. *Nucleic Acids Res.*, **43**, 10989–11002.
67. Robert,X. and Gouet,P. (2014) Deciphering key features in protein structures with the new ENDscript server. *Nucleic Acids Res.*, **42**, W320–W324.
68. Bujnicki,J.M. (1999) Comparison of protein structures reveals monophyletic origin of the AdoMet-dependent methyltransferase family and mechanistic convergence rather than recent differentiation of N4-cytosine and N6-adenine DNA methylation. *In Silico Biol.*, **1**, 175–182.
69. Randau,L., Stanley,B.J., Kohlway,A., Mechta,S., Xiong,Y. and Söll,D. (2009) A cytidine deaminase edits C to U in transfer RNAs in Archaea. *Science*, **324**, 657–659.
70. Hirata,A., Nishiyama,S., Tamura,T., Yamauchi,A. and Hori,H. (2016) Structural and functional analyses of the archaeal tRNA $m^2G/m^2{}_2G10$ methyltransferase aTrm11 provide mechanistic insights into site specificity of a tRNA methyltransferase that contains common RNA-binding modules. *Nucleic Acids Res.*, **44**, 6377–6390.
71. McCleverty,C.J., Hornsby,M., Spraggon,G. and Kreusch,A. (2007) Crystal structure of human Pus10, a novel pseudouridine synthase. *J. Mol. Biol.*, **373**, 1243–1254.
72. Somme,J., Van Laer,B., Roovers,M., Steyaert,J., Versées,W. and Droogmans,L. (2014) Characterization of two homologous 2′-*O*-methyltransferases showing different specificities for their tRNA substrates. *RNA*, **20**, 1257–1271.
73. Ozanick,S.G., Bujnicki,J.M., Sem,D.S. and Anderson,J.T. (2007) Conserved amino acids in each subunit of the heteroligomeric tRNA m^1A58 Mtase from Saccharomyces cerevisiae contribute to tRNA binding. *Nucleic Acids Res.*, **35**, 6808–6819.
74. Droogmans,L., Roovers,M., Bujnicki,J.M., Tricot,C., Hartsch,T., Stalon,V. and Grosjean,H. (2003) Cloning and characterization of tRNA (m^1A58) methyltransferase (TrmI) from *Thermus thermophilus* HB27, a protein required for cell growth at extreme temperatures. *Nucleic Acids Res.*, **31**, 2148–2156.
75. Bourgeois,G., Létoquart,J., van Tran,N. and Graille,M. (2017) Trm112, a protein activator of methyltransferases modifying actors of the eukaryotic translational apparatus. *Biomolecules*, **7**, 7.
76. Chen,C., Huang,B., Anderson,J.T. and Byström,A.S. (2011) Unexpected accumulation of ncm^5U and ncm^5S^2U in a trm9 mutant suggests an additional step in the synthesis of mcm^5U and mcm^5S^2U. *PLoS One*, **6**, e20783.
77. Patil,A., Dyavaiah,M., Joseph,F., Rooney,J.P., Chan,C.T., Dedon,P.C. and Begley,T.J. (2012) Increased tRNA modification and gene-specific codon usage regulate cell cycle progression during the DNA damage response. *Cell Cycle*, **11**, 3656–3665.
78. Figaro,S., Wacheul,L., Schillewaert,S., Graille,M., Huvelle,E., Mongeard,R., Zorbas,C., Lafontaine,D.L. and Heurgué-Hamard,V. (2012) Trm112 is required for Bud23-mediated methylation of the 18S rRNA at position G1575. *Mol. Cell Biol.*, **32**, 2254–2267.
79. Metzger,E., Wang,S., Urban,S., Willmann,D., Schmidt,A., Offermann,A., Allen,A., Sum,M., Obier,N., Cottard,F. *et al.* (2019) KMT9 monomethylates histone H4 lysine 12 and controls proliferation of prostate cancer cells. *Nat. Struct. Mol. Biol.*, **26**, 361–371.
80. Figaro,S., Scrima,N., Buckingham,R.H. and Heurgué-Hamard,V. (2008) HemK2 protein, encoded on human chromosome 21, methylates translation termination factor eRF1. *FEBS Lett.*, **582**, 2352–2356.
81. Torres,A.G., Reina,O., Stephan-Otto Attolini,C. and Ribas de Pouplana,L. (2019) Differential expression of human tRNA genes drives the abundance of tRNA-derived fragments. *Proc. Natl. Acad. Sci. U.S.A.*, **116**, 8451–8456.